8 Recent instruments and algorithms for passive shortwave remote sensing

Lorraine A. Remer, Colette Brogniez, Brian Cairns, N. Christina Hsu, Ralph Kahn, Piet Stammes, Didier Tanré, Omar Torres

8.1 Introduction

Passive remote sensing of aerosol using the shortwave spectrum draws on a long heritage of experience that began with three main techniques described in Chapter 7: occultation methods, dark target approaches, and spectral ultra-violet (UV) algorithms. Beginning in the 1970s, these techniques have been applied to instruments flown on a series of different satellite platforms and have produced important time series of aerosol parameters that span decades. This heritage is especially valuable given the fact that the early downward-viewing sensors used for aerosol retrieval – the Advanced Very High Resolution Radiometer (AVHRR), the Total Ozone Mapping Spectrometer (TOMS) and even the Geostationary Operational Environmental satellites (GOES) – were designed for purposes other than retrieving aerosol. However, the success of using these instruments for aerosol characterization motivated the development of sensors designed with aerosol retrievals in mind. Improved spatial resolution, narrower spectral channels, increased spectral range and density, enhanced capability in terms of multiple angular views of the same scene and polarization are some of the specific improvements designed into the sensors flying during the 2000s that were intended to provide better aerosol retrievals than AVHRR and TOMS.

There is no clear-cut division between heritage sensors and 'modern' sensors in terms of time period, as seen in Figure 8.1. The occultation instruments (SAM2, SAGE, SAGE2, SAGE3, HALOE, POAM2 and POAM3) have been making a continuous data record that overlaps specific sensors from 1979 to 2006, thus neatly bridging from the heritage era of the 1970s and 1980s to the modern era of the 2000s. The AVHRR aerosol record spans 1978 to the present and TOMS aboard first NIMBUS 7 and then EarthProbe (EP) begins

J. Lenoble et al. (eds.), *Aerosol Remote Sensing*, Springer Praxis Books,
DOI 10.1007/978-3-642-17725-5_8,

in 1978 and extends with one interruption to 2006. This chapter introduces some of the sensors and aerosol algorithms that are creating operational data records in the 2000s. By 'operational' it is implied that the sensors, algorithms, products and validation are supported by various space agencies for use by the entire research community, public agencies, applied scientists, the press and even average citizens. Not described in this chapter are the geostationary sensors, the Advanced Along Track Scanning Radiometer (AATSR), MEdium Resolution Imaging Spectrometer (MERIS) and the Sea-viewing Wide Field of view Sensor (SeaWIFS), even though these sensors have produced aerosol products into the same time period.

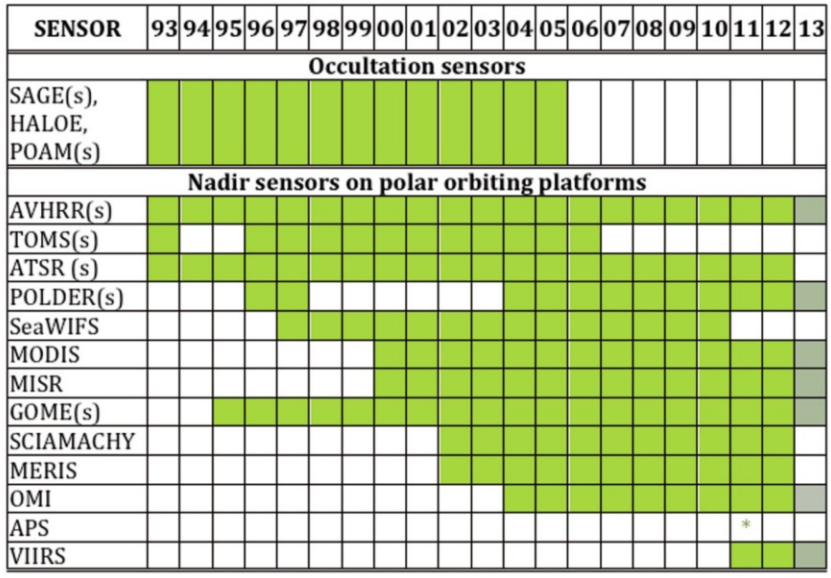

Figure 8.1 Time line of passive satellite sensors providing aerosol retrievals grouped into occultation sensors that observe stratospheric and upper tropospheric aerosol and nadir-viewing sensors aboard polar orbiting satellites. The time line begins in 1993, although the occultation sensors, AVHRR, TOMS and ATSR began contributing before 1993 and as early as 1978. Sensors still functional as of 2012 and expected to continue operating show extended functionality as gray boxes in 2013. ATSR(s), MERIS and SCIAMACHY ended their operation in April 2012 when their platform, ENVISAT, lost communication and ended its mission. VIIRS was successfully launched in October 2011. APS, the Aerosol Polarimetric Sensor, was launched in March 2011, but unfortunately did not reach orbit.

The geostationary sensor, GOES, produces a publicly available aerosol data record, but was not designed for aerosol retrievals and is considered a heritage instrument that is described in Chapter 7. The Spinning Enhanced Visible InfraRed Imager (SEVIRI) is another geostationary instrument, but with better aerosol capability. It is not included in this chapter because its publicly available data set (the GlobAerosol product at http://www.globaerosol.info/) is not in wide use (Thomas et al., 2009; Bulgin et al., 2011), while its research-level products are not operational (Govaerts et al., 2010; Wagner et al., 2010). AATSR is a direct descendant of ATSR and ATSR-2, which are described in Chapter 7. A detailed look at AATSR aerosol products can be found in Holzer-Popp et al. (2002), Grey et al. (2006) and in the AATSR product handbook at envisat.esa.int/handbooks/aatsr/CNTR2.htm. MERIS and SeaWIFS were primarily designed to support remote sensing of ocean ecology and not aerosol. Aerosol algorithms applied to these sensors were primarily for atmospheric correction of the imagery (see Chapter 7). Scenes with high aerosol loading were simply masked from the aerosol retrieval (Myhre et al. 2005). Recently, new algorithms have been applied to the SeaWIFS data record, which have produced a better representation of aerosol loading over oceans. These new algorithms are patterned on the MODIS aerosol retrieval over oceans, described below, but applied to an instrument with much narrower spectral range (Sayer et al., 2011).

In this chapter we provide an overview of the instruments, aerosol algorithms and products associated with several of the sensors that have produced an operational data record into the 2000s. Included in our discussion will be the occultation instruments, Stratospheric Aerosol and Gas Experiment (SAGE(s)) and Polar Ozone and Aerosol Measurements (POAM(s)). Then we survey the downward-viewing polar-orbiting sensors: the MODerate resolution Imaging Spectroradiometer, (MODIS) with its wide spectral range, the Multiangle Imaging SpectroRadiometer (MISR) applying its multiple angle looks at the same scene, the Ozone Monitoring Instrument (OMI) with its channels in the ultraviolet range, Global Ozone Monitoring Experiments (GOME(s)) and SCIAMACHY (Scanning Imaging Absorption Spectrometer for Atmospheric Chartography) with their hyperspectral capabilities, the Polarization and Anisotropy of Reflectances for Atmospheric Science coupled with Observations from a Lidar (PARASOL) with its multiangle looks and polarization, and finally the Aerosol Polarimetry Sensor (APS) offering highly accurate multiangle polarimetry. Some of these sensors are still flying and taking data at the time of this writing. Some have retired, and APS unfortunately was lost on launch in early 2011. It is included here because it still represents an interesting application of remote sensing theory laid out in Chapters 2, 3 and 5 and a reflight of a twin instrument is being considered.

Many of the 'modern' sensors are producing an operational product that is validated, archived and easily available to the public. The research and applied science communities have responded enthusiastically to the use of these data. Satellite remote sensing aerosol products are used to constrain climate models, to study the importance of heterogeneous processes in the atmospheric chemistry, to find relationships between clouds and aerosols, to quantify transport of particulates across oceans, to provide information in public health studies, and to improve air quality and visibility forecasts. Besides the operational products, exploratory new products and new capabilities are being explored, including combining information from several sensors that fly in formation. These cutting-edge research products are addressed in the last section of the chapter.

8.2 SAGE(s)-POAM(s): Occultation instruments

8.2.1 Missions and instrument description

The Stratospheric Aerosol and Gas Experiment (SAGE) series of instruments performing occultation measurements, including the SAM II experiment, began in 1978, as described in Chapter 7. These were NASA instruments and NASA experiments designed to explore the composition of the stratosphere and later the upper troposphere. SAM II operated at a unique wavelength and was dedicated to aerosol detection (McCormick et al., 1979), but the SAGE instruments, focused also on ozone measurements, were multi-channel instruments (Mauldin, 1985, Chu et al., 1989).

All SAGE experiments followed the same procedure. The pointing system tracked the center of brightness of the solar disk in azimuth, while scanning rapidly across the sun vertically relative to the Earth's limb. The scanning process was performed during the entire sunrise/sunset event enabling all tangent altitudes in the atmosphere to be sampled several times while viewing different parts of the solar disk. Transmissions were computed using the unattenuated irradiance coming from the same position on the sun (see Chapter 4). SAGE II and III fields of view are 300 arcseconds horizontally and 30 arcseconds vertically, which translates to about 0.5 km at the tangent altitude. Transmissions are grouped in boxes 1 or 0.5 km wide (for SAGE II and SAGE III, respectively) in altitude and an average transmission profile is derived along with uncertainty estimates on a 1 or 0.5 km grid. Such transmission profiles are produced in all channels.

Channel, nm	**Species contribution**
384.5	Aerosol, O_3, NO_2
448.5	Aerosol, O_3, NO_2
520.3	Aerosol, O_3, NO_2
601.2	Aerosol, O_3, NO_2, H_2O
675.6	Aerosol, O_3, NO_2
755.4	Aerosol, O_3
869.3	Aerosol, O_3, H_2O
1021.6	Aerosol, O_3
1545.2	Aerosol, CO_2, H_2O

Table 8.1 Species contribution in the SAGE III aerosol channels for the solar mode. The omnipresent contribution of the Rayleigh scattering is not indicated.

SAGE II was a spectrometer making measurements in seven channels in the 386 to 1020 nm range. It was launched in October 1984 into a 57-degree inclination orbit yielding a geographical coverage from about 80°N to 80°S. The SAGE II mission terminated in August 2005. SAGE III was an improved version of its predecessor with a CCD array detector comprising 809 pixels in the 290–1020 nm range, with a spectral resolution of about 1–2 nm. Out of these pixels only 87 were transmitted to the ground, some of them grouped in "resolved channels": 19 pixels between 433 and 450 nm dedicated to NO_2 retrieval and 10 3-pixel averages between 562 and 621nm for ozone. In addition, there is a photodiode at 1545 nm dedicated to aerosol characterization. A mobile attenuator permitted both solar and lunar occultation measurements. It was launched in December 2001 into a sun-synchronous polar orbit allowing observations in middle and high latitudes in the solar occultation mode. The SAGE III mission ended in March 2006.

Table 8.1 gives the list of the aerosol extinction channels only for the solar mode, since there is no aerosol product for the lunar mode. The main target species and interfering species are specified.

8.2.2 Algorithm description

The official solar retrieval algorithms for SAGE II and SAGE III both start with the species separation followed by the vertical inversion. Other inversion techniques exist, employing a reverse strategy, but they have been applied only to case studies or for validation purposes and have not been applied to the whole archive (Chu et al., 1989; Rusch et al.; 1998, Brogniez et al., 2002). The official algorithms for SAGE II and SAGE III follow similar approaches but are not identical (Chu et al., 1989; SAGE III ATBD, 2002). Only the main steps of the SAGE III algorithm are briefly described below.

At each wavelength the slant path optical depth (SPOD) can be considered as the sum of the SPOD of several species, and can be expressed in the general form

$$\tau^{SP}_{total}(Z_t,\lambda) = \tau^{SP}_{Ray}(Z_t,\lambda) + \sum_{i=1}^{N} \tau^{SP}_{gas-i}(Z_t,\lambda) + \tau^{SP}_{aer}(Z_t,\lambda), \tag{8.1}$$

where $\tau^{SP}_{Ray}(Z_t,\lambda)$, $\tau^{SP}_{gas-i}(Z_t,\lambda)$, and $\tau^{SP}_{aer}(Z_t,\lambda)$ are the Rayleigh (molecular), *gas-i* species and aerosol SPOD respectively, N being the number of absorbing gases at the considered wavelength. Z_t is the tangent altitude as defined in Chapter 4 and Figure 4.4. Deriving aerosol requires removing Rayleigh and gas contributions from the total SPOD.

Each SPOD can be expressed as a function of extinction as

$$\tau^{SP}(Z_t,\lambda) = 2\int_{Z_t}^{Z_{top}} \sigma_e(\lambda,Z)\, d\ell\,(\lambda,Z_t,Z), \tag{8.2}$$

where Z_{top} is the top of the atmosphere altitude, $\sigma_e(\lambda,Z)$ is the extinction coefficient, $d\ell$ is the geometric slant path between the altitudes Z and $Z+dZ$, accounting for the refraction. In case of an absorbing gas, the extinction coefficient is the product of the absorption cross-section with the number density $\sigma_e(\lambda,Z) = \sigma^g_a(\lambda,Z).n(Z)$.

The effects of refraction and the Rayleigh SPOD, $\tau_{Ray}^{SP}(Z_t, \lambda)$, are computed using temperature and pressure profiles available from the National Center for Environmental Prediction (NCEP) reanalyses. Ozone and nitrogen dioxide slant path number density profiles are first retrieved from the resolved channels using a multilinear regression technique. Aerosol SPOD is then derived in the nine channels after removal of all gas contributions using a set of spectral cross-sections. The availability of channels identified to retrieve NO_2 and O_3 enables the aerosol retrieval to avoid using a functional form for aerosol spectral variation as was necessary in the SAGE II aerosol retrieval.

The last step, the spatial inversion, employs a modified-Chahine method to derive gas number density and spectral aerosol extinction vertical profiles.

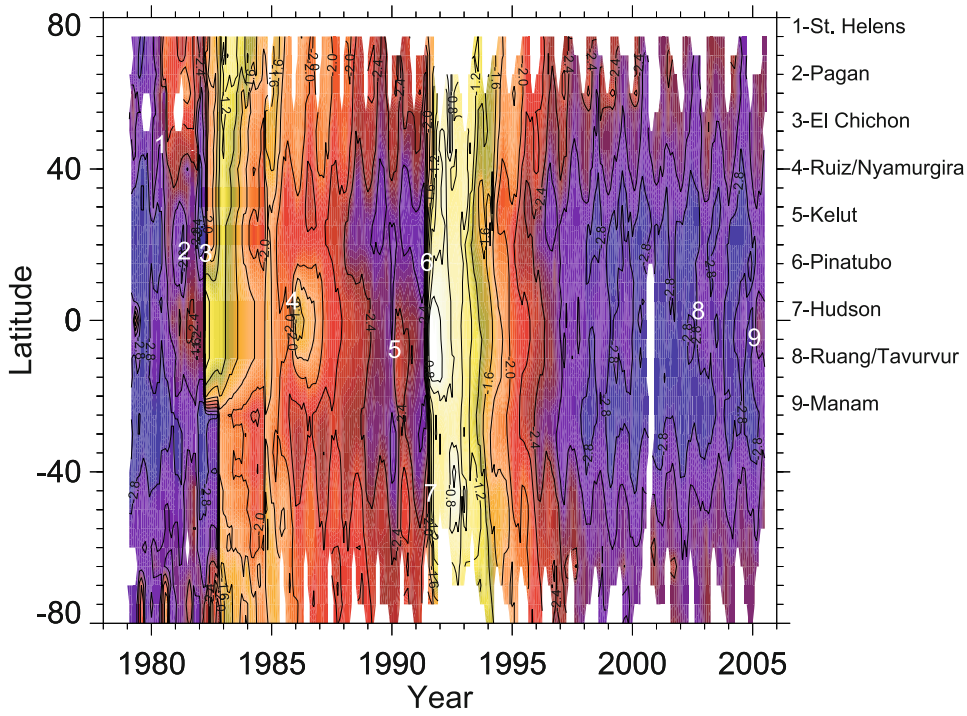

Figure 8.2 Stratospheric aerosol optical thickness ($\log_{10}$) at 1000 nm from SAM II, SAGE I, SAGE II (version 6.2) and SAGE III (version 4). The gaps due to missing observations and to El Chichon and Pinatubo's perturbations have been filled with other measurements such as lidar data following the method described in Hamill and Brogniez (2006). The main volcano eruptions are indicated. (Courtesy L. Thomason, NASA LaRc).

The retrieval algorithm provides uncertainty estimates on all products, which account for: (i) the total SPOD measurement uncertainties; (ii) the Rayleigh optical depth estimate uncertainty; and (iii) the uncertainties resulting from the removal of contributions by other interfering species. It is thus obvious that the accuracy of the products is dependent on knowledge of all gas absorption cross-sections.

Such a retrieval algorithm means that aerosol extinction coefficients are a by-product of ozone and nitrogen dioxide retrievals. Therefore, aerosols are better retrieved when the gaseous absorption contribution of the interfering species is relatively weak. This condition is not fulfilled when the aerosol loading is low, as it was during the SAGE III lifetime, making the proper choice of the gaseous cross-sections critical.

Details of the current versions of the species separation algorithms can be found for SAGE II in Thomason et al. (2001) and for SAGE III in Thomason et al. (2010).

As stated in Section 7.3, the SAGE series of instruments has permitted the establishment of the longest record of stratospheric aerosol extinction coefficient at ~1000 nm, enabling the characterization of the temporal and spatial evolution of the stratospheric aerosol loading. Figure 8.2 shows a color map contours of the derived aerosol optical depth. The gaps due to missing observations and to El Chichon and Pinatubo's perturbations have been filled with other measurements such as lidar data following the method described in Hamill and Brogniez (2006). One can clearly see that very low values (about 0.001) were occurring just before the El Chichon eruption and from 1997 up to the end of the missions (background level corresponding to periods without strong volcanic activity). On the other hand, very large values occurred following Pinatubo's eruption (0.1).

The Polar Ozone and Aerosol Measurement (POAM) II and III were developed by the Naval Research Laboratory to study the polar stratosphere (Glaccum et al., 1996). The POAM measurement procedure is different from that of SAGE as the instrument does not scan across the solar disk but stares at the center of its brightness. Then, as for the SAGE series, transmissions are computed using the unattenuated irradiance coming from the same position on the sun. The FOVs are about 3000 arcseconds horizontally and 50 arcseconds vertically, which translates to about 0.8 km at the tangent altitude. Transmission profiles are produced in all channels along with uncertainty estimates on a 1 km grid.

The POAM II instrument makes measurements in nine channels in the 352 to 1060 nm range. It was launched in September 1993 into a sun-synchronous polar orbit, yielding a geographical coverage in latitude bands about 54–71°N and 63–88°S. The POAM II mission terminated in November 1996. POAM III launched in March 1998 into an identical orbit, thus with the same latitudinal coverage, was similar to its predecessor except that the 1060 nm channel was shifted to 1020 nm, as in the SAGE II&III instruments (Lucke et al., 1997). The POAM III mission ended in December 2005.

The POAM II&III official retrieval algorithms are identical; they start with the species separation followed by the vertical inversion (Lumpe et al., 1997, 2002), as for SAGE but the technique is different. They use a nonlinear optimal estimation technique to retrieve simultaneously from the total SPOD, the gas and aerosol SPOD. For that reason they assume that the spectral variations of the aerosol SPOD follow the empirical law

$$ln\tau_{aer}^{SP}(\lambda) = \mu_0 + \mu_1 ln(\lambda) + \mu_2 (ln(\lambda))^2, \tag{8.3}$$

where μ_i are the effective aerosol coefficients to be retrieved in the algorithm. Of course, in this processing refraction effects are accounted for. The spatial inversion employs a linear optimal estimation technique to derive gas number density and spectral aerosol extinction vertical profiles. As can be seen, an important difference between SAGE III and POAM aerosol retrievals is that the former does not assume a specific spectral variation of the aerosol extinction coefficients.

HALOE, also developed by NASA, focused on several gas species (ozone, methane, HCl, H_2O...) and aerosols. The HALOE mission operated from September 1991 to November 2005 onboard the UARS platform (Russell et al., 1993). Measurements were performed in eight infrared bands and aerosol extinction coefficients were provided at four infrared wavelengths (2.45 to 5.26 μm) (Hervig et al., 1995).

8.2.3 Size distribution retrieval and derived products

Retrievals of size distribution using occultation techniques are difficult and many techniques have been developed to infer the aerosol size distribution and the higher order moments such as aerosol surface area density (SAD) or volume density and effective radius (Wang et al., 1989; Steele and Turco, 1997; Thomason et al., 1997; Anderson et al., 2000; Yue et al., 2000; Timofeyev et al., 2003; Bingen et al., 2004). The wavelength range (visible and near-infrared) of available aerosol extinction measurements limits the performances of all techniques. Indeed, the study of the sensitivity of aerosol extinction to aerosol size ranges (via kernels, see Chapter 5) shows that visible to near infrared channels provide useful information for aerosols in about the 0.1–0.8 μm range, contrarily to smaller or larger aerosols. Consequently, SAGE operational products do not include size distribution characteristics (number density and mean radius) but only higher order moments, SAD and effective radius.

The reliability of the SAD inferred from aerosol extinction coefficients depends of course on the precision of the extinction coefficients and also on the aerosol amount. Thomason et al. (2008) have shown that SAGE II SAD is poorly reliable in cases of low stratospheric aerosol loading. According to Thomason et al. (2010) SAGE III SAD should be used with caution.

8.3 MODIS/AQUA/TERRA

8.3.1 Mission and instrument description

The MODerate resolution Imaging Spectroradiometers (MODIS) were launched aboard NASA's Terra and Aqua satellites in December 1999 and May 2002, respectively. The MODIS mission is cross-disciplinary addressing the Earth System from land, ocean and atmosphere perspectives. The atmospheric focus encompasses aerosols, clouds, water vapor and atmospheric temperature soundings, the interaction between these parameters and across disciplines, especially in terms of obtaining a better understanding of how these parameters affect the Earth as a system and its climate. MODIS on Terra is collocated with

the Multiangle Imaging Spectro Radiometer (MISR) and on Aqua it flies in formation with a constellation of complementary sensors. Initially, MODIS aerosol algorithms were standalone procedures, but increasingly the advantages of combining information from several sensors are providing better retrievals and new products.

Terra crosses the equator in a descending orbit at nominal local time of 10:30 am, while Aqua crosses in an ascending orbit three hours later. Each sensor is independent, but working together the twin sensors on two different platforms with equator crossing times 3 hours apart allow for some analysis of diurnal signal, but more importantly provide a cross check on sensor calibration drift and artifacts. MODIS has 36 channels spanning the spectral range from 0.41 to 15 μm, and representing three spatial resolutions: 250 m (2 channels), 500 m (5 channels), and 1 km (29 channels). The aerosol retrieval makes use of eight of these channels (0.41–2.13 μm) to retrieve aerosol characteristics, and uses additional wavelengths in other parts of the spectrum to identify clouds and river sediments. MODIS scans cross track, observing each target at only one angle per orbit. Swath width is 2330 km, which nearly covers the globe each day and provides multiple daily views of high latitude locations.

8.3.2 Algorithm description

The MODIS aerosol algorithm is actually three separate algorithms: Dark Target over ocean, Dark Target over land and Deep Blue over land. The Dark Target algorithms over land and ocean follow from the AVHRR heritage of aerosol retrievals and are the original aerosol algorithms that were applied immediately after Terra launch. The Deep Blue algorithm is built on the SeaWiFS heritage and was implemented in 2006.

The Dark Target Ocean algorithm is aptly described in Tanré et al. (1997) and Levy et al. (2003) with updates in Remer et al. (2005). It is based on translating the elevated apparent reflectance of a dark surface target into aerosol information. Following Tanré et al. (1996), we know that the six reflectances measured from MODIS and used in the ocean retrieval (0.55–2.13 μm) contain three pieces of information about the aerosol. From this information we derive three parameters: the optical thickness at one wavelength ($\tau_{0.55}^{tot}$), the reflectance weighting parameter at one wavelength ($\eta_{0.55}$), which is defined below, and the effective radius, which is the ratio of the 3rd and 2nd moments of the aerosol size distribution. The MODIS inversion attempts to minimize the difference between the observed spectral radiance in the six MODIS channels and radiance precomputed in a look-up table (LUT). The look-up table models the total reflectance observed by satellite, which includes not only aerosol contributions, but also spatially and temporally constant atmospheric (Rayleigh) and ocean surface (chlorophyll, foam, whitecaps, and sun glint) contributions. The inversion uses the observed geometry and assumes that the total aerosol contribution is composed of a single fine and single coarse mode, and allows the inversion to choose from a set of four fine mode aerosol models and five coarse mode models. All size distributions are lognormal. The fine and coarse modes from the LUT are combined using η as the weighting parameter (Wang and Gordon, 1994),

$$\rho_{\lambda}^{LUT}(\tau_{0.55}^{tot}) = \eta\,\rho_{\lambda}^{f}(\tau_{0.55}^{tot}) + (1-\eta)\,\rho_{\lambda}^{c}(\tau_{0.55}^{tot}). \tag{8.4}$$

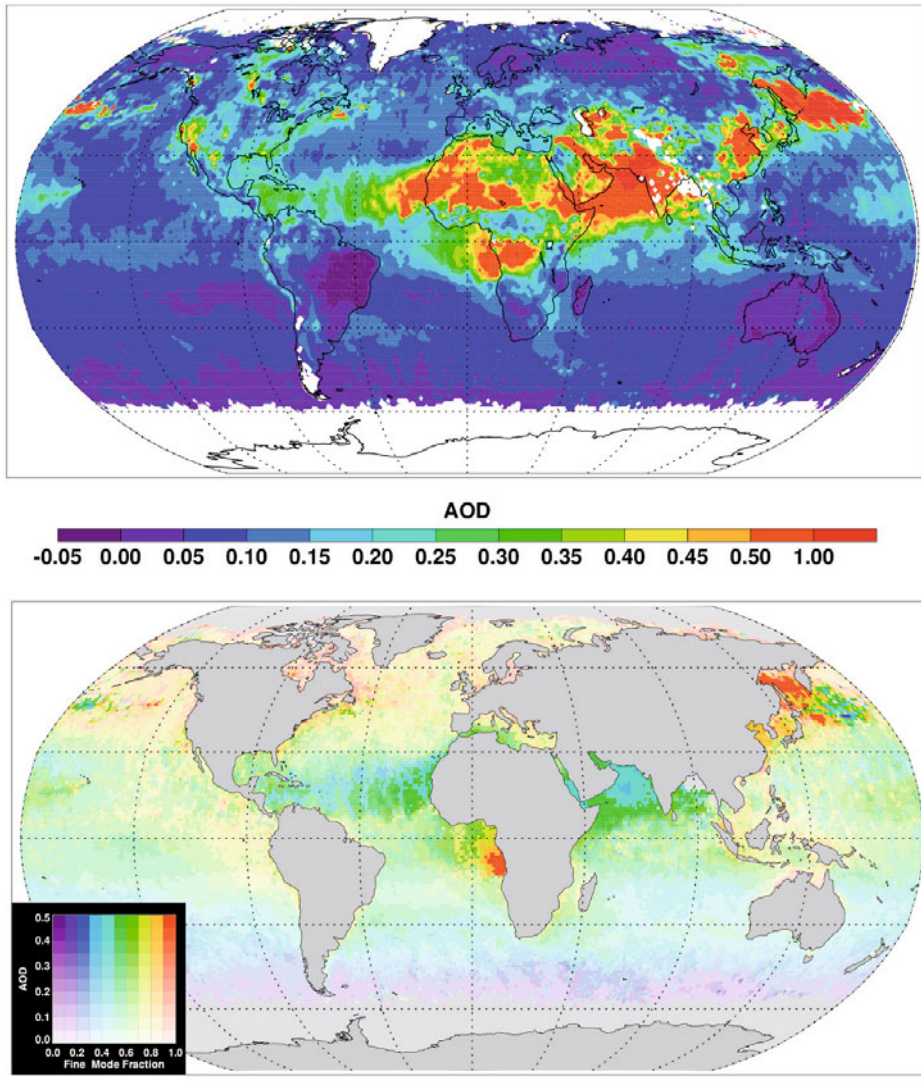

Figure 8.3 (Upper) Monthly mean aerosol optical depth from the three combined operational aerosol algorithms applied to the MODIS observations during July 2008. (Lower) Monthly mean fine fraction size parameter, η, defined in Equation 8.4 and representing the fraction of the total $\tau_{0.55}$ contributed by the fine mode component of the aerosol for July 2008. Graduations in color scale from purple to red represent changes in fine fraction from 0.0 to 1.0, respectively. Graduations in color intensity represent $\tau_{0.55}$ from 0.0 to 0.80. Size parameter products are not recommended for quantitative use when $\tau_{0.55} < 0.15$ over ocean. Size parameter products over land should be regarded as a diagnostic of the algorithm rather than a physical quantity and are therefore not shown in the lower plot.

Here "*f*" refers to fine mode and "*c*" to coarse mode, LUT refers to the reflectance from the look-up table. The spectral reflectance measured from the satellite that corresponds to the LUT value, $\rho_{\lambda}^{LUT}(\tau_{0.55}^{tot})$ for the determined values of η and $\tau_{0.55}^{tot}$, is a weighted average of the reflectance values for an atmosphere with a pure fine mode "*f*" and optical thickness $\tau_{0.55}^{tot}$ and the reflectance of an atmosphere with a pure coarse mode "*c*" also with the same $\tau_{0.55}^{tot}$. For each of the 20 combinations of one fine mode and one coarse mode, the inversion finds the pair of $\tau_{0.55}^{tot}$ and η that minimizes the differences between the measured reflectances and those from the LUT.

The Dark Target Land algorithm also compares measured reflectances against LUT values. The version used since 2006 is markedly different from the version that was first employed at Terra launch (Kaufman et al., 1997b). The current algorithm is described by Levy et al. (2007). Like the Dark Target Ocean algorithm, the land algorithm is based on retrieving aerosol optical thickness, $\tau_{0.55}^{tot}$, from the elevated apparent reflectance over a dark surface target. Over ocean, the algorithm makes simple assumptions of the spectral ocean surface reflectance. Over land, the surface reflectance is too variable for a simple assumption of reflectances. Instead, the algorithm assumes dynamical relationships between surface reflectance bands modified by geometry and the amount of vegetation in the scene. An absolute error of 0.01 of surface reflectance in a visible channel will result in an approximately 0.10 error in retrieved $\tau_{0.55}^{tot}$. The brighter the target scene, the greater the absolute error introduced into the retrieval. Even for scenes dark to our eye, some channels will be highly reflective. Thus, the retrieval restricts itself to three channels (0.47 μm, 0.66 μm and 2.13 μm) expected be relatively dark over natural land surfaces such as moist soils and vegetation. Some surfaces such as deserts, snow and ice are inherently too bright in any channel, and are avoided by the algorithm. The procedure assumes an aerosol model based on location and season, and gives some flexibility as to whether the model is fine mode dominated or coarse mode dominated. This flexibility does not translate into the same quality of information contained in the Dark Target Ocean's η parameter and should be considered a diagnostic of the algorithm and not a physical parameter. The procedure performs a simultaneous inversion of the three channels, returning $\tau_{0.55}^{tot}$ as its primary product.

The Deep Blue algorithm follows from a different heritage than the Dark Target algorithms. It is based on translating the deviation of the apparent reflectance from expected Rayleigh scattering values into aerosol information and, unlike the Dark Target approach, can be applied to bright desert surfaces and is sensitive to aerosol absorption as well as aerosol extinction. The Deep Blue algorithm takes advantage of the fact that surface reflectances over desert and semi-desert regions are much darker over the blue part of the visible light spectrum compared to the longer wavelengths. Since the optical thickness for Rayleigh scattering is much smaller at the blue wavelength compared to the UV part of the spectrum, the corresponding TOA reflectance of blue light is much less sensitive to the altitude of aerosol layers. The algorithm is applied to cloud-free scenes, mixes smoke and dust aerosol models, using a nonspherical model for dust aerosol, and bases its surface reflectance assumptions on a precalculated surface reflectance database. The algorithm makes use of the 0.412 μm, 0.490 μm, and 0.670 μm bands to provide spectral information in finding the correct mix of smoke and dust (Hsu et al., 2004). The resulting output includes both aerosol optical depth, Ångström exponent, and dust single scattering albedo.

Combining the three MODIS algorithms provides a global quantitative view of the Earth's aerosol system over most of the land and ocean regions of the Earth. Figure 8.3 shows an example of monthly mean aerosol optical depth using a combination of the three algorithms described above. Figure 8.3 also shows an example of monthly mean size parameter, η, for the same month. The size parameter is retrieved only quantitatively by the Dark Target ocean retrieval.

8.3.3 Data use considerations

Some, but not all, of the MODIS aerosol products have been compared extensively against similar measurements made by instruments with known higher accuracy. In the MODIS case, this means comparison against data measured by the AERONET instruments (see Chapter 6). By comparing with higher accuracy instruments, the uncertainty of MODIS aerosol optical depth, has been quantitatively characterized and validated (Remer et al., 2005; Levy et al., 2010). Validated does not indicate a perfect retrieval, nor does it mean an unbiased retrieval. Also, validation is performed either globally or over broad geographical regions. A specific region may introduce biases when surface conditions and/or aerosol characteristics deviate from the assumptions used in the global retrieval. Careful analysis and empirical corrections can produce an unbiased product (Zhang et al., 2008).

One significant bias not due to regional inconsistency with retrieval assumptions is the 0.015 offset between Terra and Aqua $\tau_{0.55}^{tot}$ over oceans (Remer et al., 2008). This offset has been traced to calibration issues, with Terra appearing to be too high. Other calibration issues have introduced artificial trends in the MODIS time series (Levy et al., 2010; Zhang and Reid, 2010)

While the MODIS aerosol product provides the community with well-characterized, easily accessible information on aerosols, care must be taken to consider Quality Assurance (QA) flags at all data levels. Global and regional mean statistics are sensitive to choice of aggregation procedures that translate the nominal 10 km product based on orbital geometry to the so-called Level 3 gridded 1 degree product (Levy et al., 2009). It is preferable for users to always acquire daily data and produce their own monthly means, and thereby have control over the aggregation procedures employed.

Because the MODIS aerosol product is operational, it continuously undergoes analysis and changes are implemented. Documentation on algorithm changes and errata are kept current in the MODIS Dark Target Algorithm Theoretical Basis Document (ATBD) available at http://modis-atmos.gsfc.nasa.gov/reference_atbd.html.

8.4 MISR/TERRA

8.4.1 Mission and instrument description

The Multiangle Imaging SpectroRadiometer (MISR) was launched aboard the NASA Earth Observing System (EOS) Terra spacecraft in December 1999, into a sun-synchronous orbit that crosses the equator at about 10:30 local time, descending on the day side of the planet.

It is unique among the EOS-era satellite instruments in having a combination of high spatial resolution (up to 275 m/pixel), a wide range of along-track view angles, and high-accuracy radiometric calibration (~3% absolute, ~1.5% channel-to-channel) and radiometric stability (Diner et al., 1998). Near-global coverage is obtained about once in nine days at equatorial latitudes, and about once every two days in polar latitudes up to 82°.

MISR measures upwelling short-wave radiance from Earth in four spectral bands centered at 446, 558, 672, and 866 nm, at each of nine view angles spread out in the forward and aft directions along the flight path, at 70.5°, 60.0°, 45.6°, 26.1°, and nadir. Over a period of seven minutes, as the spacecraft flies overhead, a 380-km-wide swath of Earth is successively viewed by each of MISR's nine cameras. As a result, the instrument samples a very large range of scattering angles – between about 60° and 160° at mid latitudes – providing information about aerosol microphysical properties. These views also capture air-mass factors ranging from one to three, offering sensitivity to optically thin aerosol layers, and allowing aerosol retrieval algorithms to distinguish top-of-atmosphere reflectance contributions from the surface and atmosphere.

The MISR data are used to study Earth's surface, clouds, and aerosols. Total-column aerosol optical depth (τ) is retrieved over dark water and most land, including bright desert (Martonchik et al., 2004; Kahn et al., 2010). Sensitivity to aerosols varies with surface albedo, scene heterogeneity, and the range of scattering angles observed. As with most passive aerosol remote sensing techniques, MISR aerosol retrievals are not obtained under cloudy conditions, over complete snow or ice cover, mountainous terrain, and some coastal regions (Case 2 waters), where runoff, pollution, biological activity, or shallow water make the ocean surface reflective in the MISR red and near-infrared wavelengths. A description of the MISR aerosol algorithm quality flags, and comparisons with near-coincident MODIS retrievals of τ and Ångström exponent, is given by Kahn et al. (2009a).

At least over dark water, for good but not necessarily ideal viewing conditions (i.e. cloud-free, mid-visible τ larger than about 0.15, adequate range of scattering angles), MISR can also distinguish about 3–5 groupings based on particle size, 2–4 groupings in single-scattering albedo (SSA), spherical vs. nonspherical particles, and thin cirrus from most types of aerosol (Chen et al., 2008; Kahn et al., 2001; Kalashnikova and Kahn, 2006; Pierce et al., 2010). In addition, MISR stereo height retrievals are used to obtain aerosol injection height in the source regions for wildfire smoke, desert dust, and volcanic plumes, where there are sufficient contrast-features in the plumes to perform multiangle image matching (Kahn et al., 2007).

8.4.2 Algorithm description

The MISR Standard Aerosol Retrieval algorithm runs in an operational, fully automatic mode. It reports τ and aerosol type derived over 17.6×17.6 km retrieval regions, by analyzing the MISR top-of-atmosphere radiances measured in the 16×16 1.1 km sub-regions within each region (Martonchik et al., 1998; 2002). Separate algorithms are applied to observations taken over dark water and over heterogeneous land. Both aerosol retrieval algorithms can be divided into three stages (Diner et al., 2006). Stage 1 involves pre-processing the radiometrically and geometrically calibrated radiances, and performing out-of-band spectral, ozone and water vapor absorption corrections. In addition, screening is performed

in Stage 1 for missing radiance data, complex terrain over land, low solar-zenith-angle cases, sun-glint-contaminated views over water, and cloudy locations; the remaining radiance data are converted to equivalent reflectances. In Stage 2 of the processing, the type of algorithm used to perform the retrieval (land or water) is determined based on the data that pass the Stage 1 tests. Finally, in Stage 3, acceptance criteria are used to identify simulated top-of-atmosphere equivalent reflectances from look-up tables that match those observed by the instrument.

The land–water differences are most prominent in Stage 2 of the algorithm, after acceptable retrieval regions have been selected. Over water, only the red and near-infrared channels are used, to minimize water reflectance. The dark ocean surface is modeled as a Fresnel reflector, with standard, wind-dependent surface roughness and whitecap models;

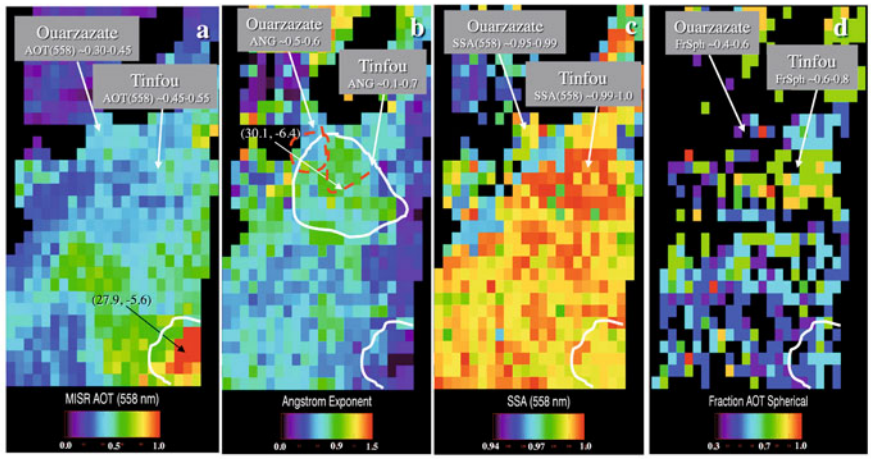

Kahn et al., Tellus 2009

Figure 8.4 MISR Standard aerosol retrieval products acquired on 04 June 2006 at 11:11 UTC, over the SAMUM Field Campaign ground sites at Ouarzazate and Tinfou, Morocco. (a) Mid-visible Aerosol Optical Thickness; (b) Ångström exponent; (c) Mid-visible Single-scattering albedo (SSA); (d) Fraction Optical Thickness of Spherical particles. A dust-laden density flow appears in the southeast (lower right) corner of these images, and an airmass containing higher SSA, higher Ångström exponent (smaller), spherical particles compared to the background desert aerosol is found at the center of the region, outlined in white in panel (b). The dashed red line in this panel traces the flight of the DLR Falcon F20, which verified the presence of two thin layers of small, spherical particles in the highlighted region; back-trajectories indicate that this represents pollution particles transported from the Algerian coast. (From Kahn et al., 2009b. Reprinted with permission from the International Meteorological Institute in Stockholm)

in initial processing, near-surface winds are adopted from a monthly, global climatology whereas about one month after data acquisition, the retrievals are rerun using measured winds.

The over-land algorithm is a two-step process, both of which are intrinsically multiangle (Martonchik et al., 2009). In Step 1, the idea that the angular signature of surface reflectance is approximately spectrally invariant is used to filter out those aerosol mixtures from among those assumed in the algorithm that grossly disagree with the observed radiances (Diner et al., 2005). In Step 2, a principal components analysis is performed on the available multiangle, multi-spectral top-of-atmosphere (TOA) MISR radiances (Martonchik et al., 1998). A scatter matrix is constructed as the sum over all sub-regions within the 17.6 km retrieval region that pass the Stage 1 tests, of camera-by-camera differences between TOA equivalent reflectances:

$$C_{\lambda}(i,j) = \sum_{x,y}\left[L^{MISR}_{x,y,\lambda}(i) - L^{MISR}_{bias,\lambda}(i)\right]\left[L^{MISR}_{x,y,\lambda}(j) - L^{MISR}_{bias,\lambda}(j)\right], \tag{8.5}$$

where i and j are camera indices, x and y are spatial indices, λ is the wavelength index, L are the TOA reflectances, and the "*bias*" subscript references the camera and band-appropriate reflectances for the sub-region within the retrieval region having the darkest green-band reflectance. As the atmosphere is assumed homogeneous over the retrieval region field-of-view (taking account of angular viewing), the atmospheric path radiance cancels from each term, and the scatter matrix depends only on surface properties. Scene contrast must be sufficient to effect this surface–atmosphere separation. The spatially dependent surface reflectance contribution is then constructed from the EOFs and eigen values of the C matrix, and the atmospheric path radiance is obtained as the difference between the MISR TOA reflectances and the calculated surface contribution. The optical depth is determined to minimize the difference between the observed and reconstructed reflectances. This process is repeated for all mixtures that pass the angular similarity filter of Step 1, and all those that meet the acceptance criteria are reported as matching the observations to within the sensitivity of the measurements.

Critical to the success of this process is providing the algorithm with aerosol component optical models and mixture options that reflect those commonly found in the atmosphere, at a level-of-detail appropriate to the sensitivity of the measurements. A combination of theoretical sensitivity studies, field campaign results, and statistical comparisons with surface validation data, stratified by expected aerosol type, has been used to develop the aerosol component and mixture climatology (Kahn et al., 2001; 2005, 2009b; Chen et al., 2008; Kalashnikova and Kahn, 2006]. At least two-thirds of MISR-retrieved aerosol optical depths fall within 0.05 or 20% of coincident validation values, whichever is larger. Sensitivity to particle size, shape, and SSA varies with conditions. So aerosol air mass type, a classification based on the aggregate of MISR particle microphysical property constraints, is being investigated as a robust way to summarize the retrieved aerosol type information. The limited particle property validation data available indicate that about a dozen aerosol air mass types can be distinguished from the MISR data under good observing conditions. Aerosol type discrimination, in a situation where field data were available for validation,

is illustrated in Figure 8.4, and references to a range of aerosol applications papers that use the MISR data are given in Kahn et al. (2011). Improvements to the Version 22 MISR aerosol product, including the addition of medium-mode and more absorbing aerosol components, as well as mixtures of smoke and dust analogs missing from the current algorithm climatology but common at some locations in some seasons, are planned for future product releases (Kahn et al., 2010).

8.5 POLDER/PARASOL

8.5.1 Mission and instrument description

The PARASOL (Polarization and Anisotropy of Reflectances for Atmospheric Science coupled with Observations from a Lidar) mission (Tanré et al., 2011) is the second in CNES's Myriade (Centre National d'Études Spatiales) line of microsatellites. PARASOL was launched on December 18, 2004 and was part of the A-Train. It was in a sun-synchronous orbit at an altitude of 705 km with 1:30 pm equator-crossing time on the ascending node and has been routinely acquiring data since March 2005. The payload (Deschamps et al., 1994) consists of a POLDER-like digital camera with a 274x242-pixel CCD detector array, wide-field telecentric optics and a rotating filter wheel enabling measurements in nine spectral channels from blue (0.443 μm) through to near-infrared (1.020 μm) and in several polarization directions at 0.490 μm, 0.670 μm and 0.865 μm. The bandwidth is between 20 nm and 40 nm depending on the spectral band. As it acquires a sequence of images every 20 seconds, the instrument can view ground targets from different angles, +/– 51° along track and +/– 43° across track. Because of limited on-board fuel budget, the PARASOL orbit was decreased by 4 km at the end of 2009. The drift of the orbit since 2009 has resulted in a crossing time of around 2:30pm at the end of 2011.

8.5.2 Algorithm description

Over ocean, the inversion scheme uses the total normalized radiances in the 670 nm and 865 nm channels only, to avoid the contamination by the ocean reflectance that is very variable at 555 nm and in the blue region. The polarized Stokes parameters at 865 and 670 nm are also used for deriving the best aerosol model. The rough ocean is modeled with the Cox and Munk (1954) equations assuming a wind speed of 5 m/s for considering the surface–atmosphere multiple interactions. The actual wind speed provided by the ECMWF weather forecast model is used in the glint mask and for computing the foam reflectance. The foam coverage is calculated according to the Koepke's model (1984) with a reflectance of 0.22 at both wavelengths. The underwater contribution is taken equal to 0.001 and 0.000 at 670 and 865 nm respectively. Let us add that PARASOL has always at least one viewing direction out of the glint making aerosol τ retrievals possible everywhere over water.

The algorithm is based on a comparison between spectral, directional and polarized measurements and LUT built for a set of aerosol models (size distribution, refractive index, optical thickness) and for geometrical and other atmospheric conditions as close as possi-

ble to the actual situation. The aerosol size distribution is bimodal with an accumulation mode between 0.1–0.2 μm and a spherical coarse mode around 2.50 μm (Herman et al., 2005). Each mode of spherical particles follows a lognormal distribution, and several real refractive indices for each mode are considered. m = 1.35, 1.45 and 1.60 for the accumulation mode and m = 1.33, 1.35 and 1.37 for the coarse mode. Particles are considered non-absorbing in both modes. Since PARASOL measurements are sensitive to the shape of aerosols, a model of nonspherical dust is included in the LUT. The phase matrix is taken from Volten et al. (2001) and the model assumes no spectral dependence. Concerning its physical properties, the effective radius is taken equal to 2.50 μm and there is no retrieval of the refractive index of the coarse mode in presence of dust. The dust can be mixed with the spherical coarse mode through 5 values: 0.00, 0.25, 0.50, 0.75 and 1.00. The LUTs are built using the Successive Order of Scattering (SOS) method (Chapter 3) including polarization computations (Lenoble at al., 2007). The radiances as well as the normalized Stokes parameters Q and U are pre-computed following Eq. 8.4.

Limitations:

- For low aerosol content , the aerosol model is fixed and only the aerosol optical thickness is derived.
- The refractive indices and modal radii of the small and large spherical particles are not derived everywhere since the retrieval requires a scattering angle coverage larger than 125°–155°, which depends on the viewing conditions for a given pixel.

Over land, aerosol remote sensing from solar radiance measurements is more difficult than over ocean because the reflectance from the surface is generally much larger than the reflectance from aerosols at the top of the atmosphere, except over dark surfaces such as vegetation in the blue part of the solar spectrum (see Section 8.3). The use of polarized radiances is very attractive in such conditions. Airborne experiments have shown that the relative contribution of the surface compared to the atmosphere, is less important in polarized light than in total light (Deuzé at al., 2001), which makes the polarized satellite radiances more subject to the presence of aerosols than the total radiances. In addition, contrary to the total radiances, polarized radiances reflected by terrestrial surfaces are fairly spectrally independent and uniform. The surface contribution in the POLDER algorithm is then handled in the following way: (i) two surface models are considered, bare soils and vegetated areas, and (ii) the contribution is then estimated from a relationship using empirical coefficients adjusted for the different classes of land surfaces according to the main IGBP biotypes and the NDVI (Nadal and Bréon, 1999). Nevertheless, there is a drawback using polarization that comes from its deficiency to detect all types of particles. Large particles do not polarize sunlight and, for instance, desert dust is not accessible for a quantitative inversion. Aerosol polarization mainly comes from the small spherical particles with radii less than about 0.5 μm. So, the present algorithm over land, based on a best fit between polarized measurements at 670 and 865 nm and LUTs, retrieves aerosols within the accumulation mode only. So, particles within the coarse mode are not considered in the LUT. They are computed for 10 effective radius (from 0.075 to 0.225 μm) of the fine mode with a complex refractive index equal to 1.47–0.01i, which corresponds to a mean value for aerosols resulting from biomass burning or pollution events (Dubovik et al., 2002).

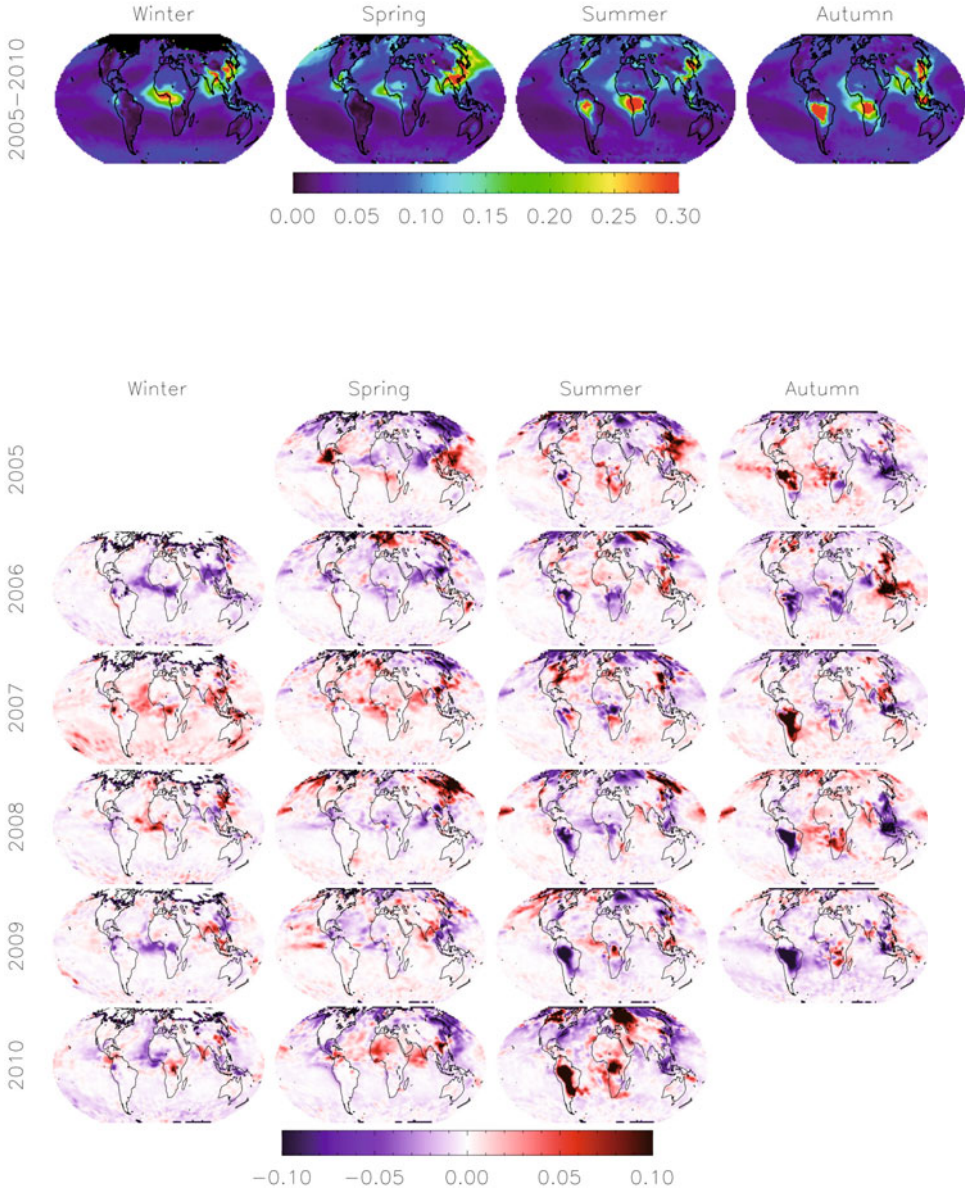

Figure 8.5 Top panel: AOD at 550 nm resulting from the accumulation mode for the 4 seasons averaged over 6 years. Bottom panel: AOD anomalies for the six years from 2005 to 2010. Blues indicate that the AOD of the year was lower than the long term mean and reds indicate higher values.

Limitations:

- Surface models are less accurate over deserts near the horizon.
- The coarse mode can contribute to the polarization for very intense events that are difficult to identify.

Figure 8.5 illustrates the capabilities of the sensor to derive the aerosol optical depth of the accumulation mode over land and ocean. It is a very important parameter since aerosol types dominated by the fine mode are mostly the result of combustion activity and consequently anthropogenic (Kaufman et al., 2005). In Figure 8.5, aerosol optical thickness anomalies for six years are compared with the 2005–2010 mean values (top panel) for the four seasons. The top panel illustrates the large seasonal variability of the source regions. In the autumn season, high values of the AOD are reported over Brazil, South Africa and Indonesia due to fires. High values are observed in the Indo-Gangetic Plain of India and eastern China during all seasons. In summer, North America and Europe display moderate aerosol loading. Biomass burning occurs again in Africa, north of the equator, in winter, and in Central America during the spring. The bottom panel in Figure 8.5 shows the yearly evolution with important variations in specific regions and seasons. The causes of the fluctuations are multiple: (i) changes in intensity and number of fires or controls of pollutant emissions; (ii) changes in meteorological fields that affect aerosol transport; or (iii) changes in scavenging processes, precipitations or dry deposition.

8.5.3 Advanced POLDER retrieval

A new algorithm for enhanced retrievals of aerosol properties from POLDER/PARASOL observations is under development As illustrated in Kokhanovsky et al. (2010) using synthetic data, PARASOL-like measurements combined with a sophisticated inversion algorithm (Dubovik et al., 2011) are the most accurate means for retrieving the aerosol properties when compared with other algorithms and sensors.

Indeed, PARASOL observations form the most comprehensive data set currently available from space, which provides an opportunity for a deeper utilization of statistical optimization principles in satellite data inversion. The retrieval is designed as a statistically optimized multi-variable fitting of the complete PARASOL observation set, including both measurements of total radiances and polarized at all available spectral channels (Dubovik et al., 2011). Based on this strategy, the algorithm is driven by a larger number of unknown parameters and aimed at a retrieval of an extended set of parameters affecting measured radiation. For example, this approach allows the retrieval of both the optical properties of the aerosol and the underlying surface from PARASOL observations over land. Also, the algorithm is expected to provide more detailed (compared with the current operational PARASOL algorithm) information about aerosol properties over land including some information about aerosol sizes, shape, absorption and composition (refractive index).

In addition, the algorithm was inspired by the MAIAC inversion for MODIS (Section 8.9.2), and is developed as a simultaneous inversion of a large group of pixels within one or several images. Such a multi-pixel retrieval regime is expected to take advantages of known limitations on spatial and temporal variability in both aerosol and surface properties. Specifically, the pixel-to-pixel or day-to-day variations of the retrieved parameters

are forced to be smooth by imposing additional appropriately set *a priori* constraints. We anticipate higher consistency in the retrievals because the retrieval over each single pixel will be benefiting from co-incident aerosol information from neighboring pixels, as well as from the information about surface reflectance (over land) obtained in preceding and consequent observation over the same pixels.

This new inversion procedure has been applied to a limited PARASOL data set. The method is very promising since retrievals of the total AOD over bright surfaces like deserts have been performed and show good agreement with coincident AERONET measurements over Banizoumbou, Niger (Dubovik et al., 2011).

8.6 OMI-Aura

8.6.1 Mission and instrument descriptions

The Ozone Monitoring Instrument (OMI) is one of four sensors on the EOS-Aura platform launched on July 15, 2004 (Schoeberl et al., 2006). The Aura spacecraft is part of the A-train, a set of satellites flying in close proximity. Other A-train aerosol sensors are Aqua-MODIS (aerosol component described above), PARASOL (described above), and CALIOP (Chapter 10). Aura's equator crossing time changed from 13:45 at launch to 13:38 in May 2008 to reduce the time difference of the observation with other A-train sensors. The OMI project (Levelt et al., 2006) is an international effort that involves the participation of the Netherlands, Finland, and the USA. OMI is a high spectral resolution spectrograph that measures the upwelling radiance at the top of the atmosphere from the ultraviolet to the visible (270–500 nm). It has a 2600 km wide swath and provides daily global coverage at a spatial resolution varying from 13×24 km at nadir to 28×150 km at the extremes of the swath. The OMI sensor was designed to map on a daily basis the global distribution of the total atmospheric ozone content and its vertical distribution. The hyper-spectral nature of OMI observations allows the application of techniques to derive the atmospheric content of other important trace gases such as NO_2, SO_2, HCHO, BrO, etc. (Platt, 1994). OMI observations are also used for the estimation of cloud heights, and for the characterization of atmospheric aerosols, which will be described below.

8.6.2 Algorithms description

Two aerosol inversion schemes are applied to the OMI measurements; the OMI near-UV (OMAERUV) algorithm uses two UV wavelengths to derive aerosol extinction and absorption optical depth. A multi-wavelength algorithm (OMAERO) that uses up to 19 channels in the 330–500 nm spectral range is used to derive aerosol extinction optical depth at several wavelengths.

Near UV aerosol algorithm (OMAERUV)

The OMAERUV algorithm makes use of two major advantages of the near-UV spectral region for deriving aerosol properties. The reflectance of all terrestrial surfaces (not covered

with snow) is small in the UV and, therefore, the retrieval of aerosol properties is possible over a larger variety of land surfaces than in the visible, including the arid and semi-arid regions of the world that appear very bright in the visible and near-IR. The second advantage is the strong interaction between aerosol absorption and molecular scattering from below the aerosol layer that allows one to estimate the aerosol absorption capacity of the atmospheric aerosols (Torres et al., 1998, 2005). The OMAERUV algorithm is an application to the OMI observations of the near-UV technique of aerosol detection and characterization developed based on observations by the TOMS sensor and discussed in detail in Chapter 7.

The OMAERUV aerosol algorithm uses measurements at 354 nm and 388 nm to retrieve aerosol extinction optical depth and single scattering albedo at 388 nm. In addition to these parameters, the UV Aerosol Index (UVAI) is calculated as described in Section 7.5.1 for $\lambda = 354$ nm and $\lambda_0 = 388$ nm.

Aerosol Index

The first step in the derivation of the Aerosol Index is the calculation of the Lambertian reflectivity R_{388} using Eq. 7.6. The quantity R_{388} is usually larger than the true surface reflectivity, R_{388}^{sfc}, due to scattering from clouds and aerosols but it can be smaller if the aerosols are highly absorbing. The term R_{354} is estimated by correcting R_{388} for the spectral dependence of the actual surface reflectivity,

$$R_{354} = R_{388} + [R_{388}^{sfc} - R_{354}^{sfc}], \tag{8.6}$$

using a pre-computed climatological database of surface reflectivity in the 331-380 nm spectral region obtained from TOMS multi-year observations similar to that of Herman and Celarier (1997). The calculated top of the atmosphere 354 nm radiance associated with the adopted surface-atmosphere model representation, as given by

$$L_{354}^{cal} = L_{354}^{0} + \frac{R_{354} T_{t\_354}}{1 - S_{354} R_{354}}, \tag{8.7},$$

is then used in the computation of the OMI UV aerosol index, AI,

$$\mathrm{AI} = -100 \log\left[\frac{L_{354}^{\mathrm{M}}}{L_{354}^{cal}}\right], \tag{8.8}$$

where L^{M}_{354} is the satellite observed radiance at 354 nm. All parameters on the right side of Eq. (8.7) are defined in Chapter 7.

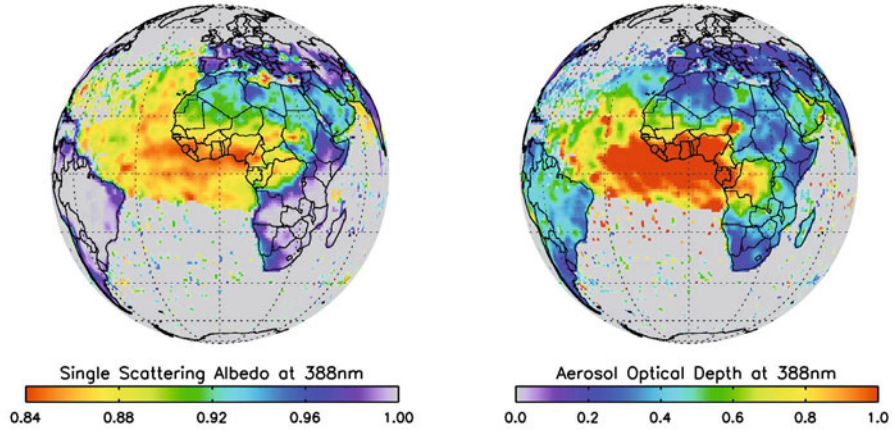

Figure 8.6 OMAERUV January 2007 monthly average aerosol optical depth and single scattering albedo.

Aerosol extinction optical depth and single scattering albedo

Aerosol extinction optical depth and single scattering albedo at 388 nm are derived using a standard inversion algorithm that uses pre-computed reflectances for a set of assumed aerosol models. The retrieval algorithm is in many ways similar to the one applied to TOMS observations (Torres et al., 2002). Three major aerosol types are considered: desert dust, carbonaceous aerosols associated with biomass burning, and weakly absorbing sulfate-based aerosols. The carbonaceous aerosol model accounts for the presence of black and organic carbon as the main light absorbing components (Jethva and Torres, 2011). Each aerosol type is represented by seven aerosol models of varying single scattering albedo, for a total of 21 microphysical models (Torres et al., 2007). In the current algorithm version, the selection of the aerosol type is carried out based on spectral considerations and the use of ancillary information available from other sensors. The separation of absorbing and non-absorbing aerosols is done by means of the AI concept. Carbonaceous aerosols are differentiated from desert dust aerosols making use of the observed correlation between the AI and the CO column amount product of the Aqua-AIRS sensor.

For a chosen aerosol type, represented by a subset of seven aerosol models, the extinction optical depth and single scattering albedo are retrieved by examining the variability of the 354–388 nm radiance ratio spectral contrast and the 388 nm reflectance. Since the

retrieved parameters are sensitive to the aerosol layer height, the altitude of the absorbing aerosol layer must be prescribed. OMAERUV uses a global monthly climatological data set of aerosol height derived from CALIOP observations.

Given the relatively large size of the OMI pixels (compared to sensors specifically designed for aerosol retrieval, such as MODIS), OMI pixels are often cloud contaminated. The effect of sub-pixel cloud contamination is the overestimation of the extinction optical depth and underestimation of the single scattering co-albedo (Torres et al, 1998) and, therefore, a partial cancellation of sub-pixel cloud contamination errors takes place in the calculation of the aerosol absorption optical depth (AAOD). Thus, AAOD results are still reliable even in the presence of small amounts of cloud contamination. OMAERUV retrieval results have been evaluated using airborne (Livingston et al., 2009), and ground-based (Torres et al., 2007) sun-photometer measurements and by comparison to MODIS and MISR observations (Ahn et al., 2008).

Figure 8.6 shows the January 2007 monthly averages of retrieved aerosol single scattering albedo and extinction optical depth over Africa and the Atlantic Ocean. Aerosol optical depth values larger than unity from biomass burning activity cover the Tropical Atlantic. Much lower values are observed over the Saharan desert and the North Atlantic where desert dust aerosols are present. Single scattering albedo values as low as 0.82 are associated with the smoke layer whereas values in the vicinity of 0.92 are observed for dust aerosols.

Multi-wavelength aerosol algorithm (OMAERO)

The OMI multi-wavelength algorithm (OMAERO) is used to derive aerosol characteristics from OMI spectral reflectance measurements of cloud free scenes at up to 19 wavelengths in the spectral range between 330 nm and 500 nm (Torres et al., 2007). The sensitivity to the layer height and single scattering albedo is related to the relatively strong contribution of Rayleigh scattering to the measured reflectance in the UV (Torres et al, 1998). The absorption band of the O_2–O_2 collision complex at 477 nm is used in OMAERO to enhance the sensitivity to the aerosol layer height (Veihelmann et al., 2007) in a way similar to its use in the retrieval of cloud height (Acarreta et al., 2004). Spectral surface albedo in the UV-VIS spectral region is taken from a climatological data set produced from three years of OMI observations (Kleipool et al., 2008).

Aerosol parameters are determined by minimizing the merit function Ψ_m,

$$\Psi_m = \sum_{i=1}^{N} \left(\frac{L^*(\lambda_i) - L_m(\tau(\lambda_{ref}), \lambda_i)}{\varepsilon(\lambda_i)} \right)^2, \tag{8.9}$$

where $L^*(\lambda_i)$ is the measured reflectance, $L_m(\tau(\lambda_{ref}), \lambda_i)$ is the reflectance for the aerosol model m as a function of the aerosol optical thickness τ at the reference wavelength λ_{ref}, and $\varepsilon(\lambda_i)$ is the error in the measured reflectance. The merit function is a sum over N wavelength bands. An optimal τ is determined for each model by a non-linear fitting routine using a modified Levenberg-Marquardt method (Moré, 1978). The best fitting aerosol model with the smallest Ψ_m is selected for the present ground pixel. The retrieved AOD value and

precision of the best fitting aerosol model are provided in the OMAERO product. Also, the values of single-scattering albedo, size distribution and aerosol height that are associated with the best fitting aerosol model are provided.

8.7 GOME-SCIAMACHY

8.7.1 Instrument description

GOME (Global Ozone Monitoring Experiment) and SCIAMACHY (Scanning Imaging Absorption Spectrometer for Atmospheric Chartography) are satellite spectrometers measuring reflected sunlight. Although these instruments are intended for measuring trace gases like O_3, NO_2, CO, and CH_4, and have limited spatial resolution, some of their characteristics, like contiguous spectral coverage from UV to near-IR, inclusion of O_2 A-band, and polarization channels, give them unique aerosol observational capabilities. Furthermore, the combination of trace gas and aerosol measurements may lead to a better understanding of the formation of secondary aerosols.

SCIAMACHY flies on the European Space Agency's (ESA's) Envisat satellite, launched in March 2002. SCIAMACHY is a grating spectrometer with eight spectral channels covering the range 240–2380 nm. The spectral resolution varies from 0.2 nm in the UV to 1.5 nm in the near-IR (Bovensmann et al., 1999). SCIAMACHY has three viewing modes: nadir, limb and occultation (Sun and Moon). The ground pixel size in nadir mode is 30×60 km^2 for most wavelengths. The full spectrum is measured at 30×240 km^2 resolution. In limb mode the spatial resolution is 3×240 km^2. Both in nadir and limb mode the swath is 960 km wide. The nadir and limb modes alternate each other along the orbit, and therefore full global coverage is achieved in six days.

GOME was developed as a simpler version of SCIAMACHY, and was launched in April 1995 on the ERS-2 satellite of ESA. GOME has four spectral channels covering the range 240–790 nm with spectral resolution 0.2-0.4 nm, and has nadir mode only (Burrows et al., 1999a). Its pixel size is 40×320 km^2, and its swath is 960 km. Global coverage is achieved in three days. Due to its solid state recorder failure, GOME lost global coverage in June 2003; after that the coverage has been limited to 30–40%. The instrument and satellite were switched off in July 2011.

GOME-2 is the successor of GOME and flies on EUMETSAT's Metop-A satellite, launched in October 2006 (Callies et al., 2000). GOME-2 has 40×80 km^2 pixels and a 1920 km wide swath, providing global coverage in 1.5 days. GOME-2 has the same spectrometer capabilities as GOME, but it has enhanced polarization detectors (PMDs): its 15 spectral PMD channels, in the range 330–750 nm, for two perpendicular polarization directions enable measurement of both Stokes parameters I and Q with spatial resolution of 40×10 km^2.

The in-flight radiometric and spectral calibrations of GOME and SCIAMACHY consist of daily Sun observations (via a diffuser) and on-board lamp monitoring (Lichtenberg et al., 2006).

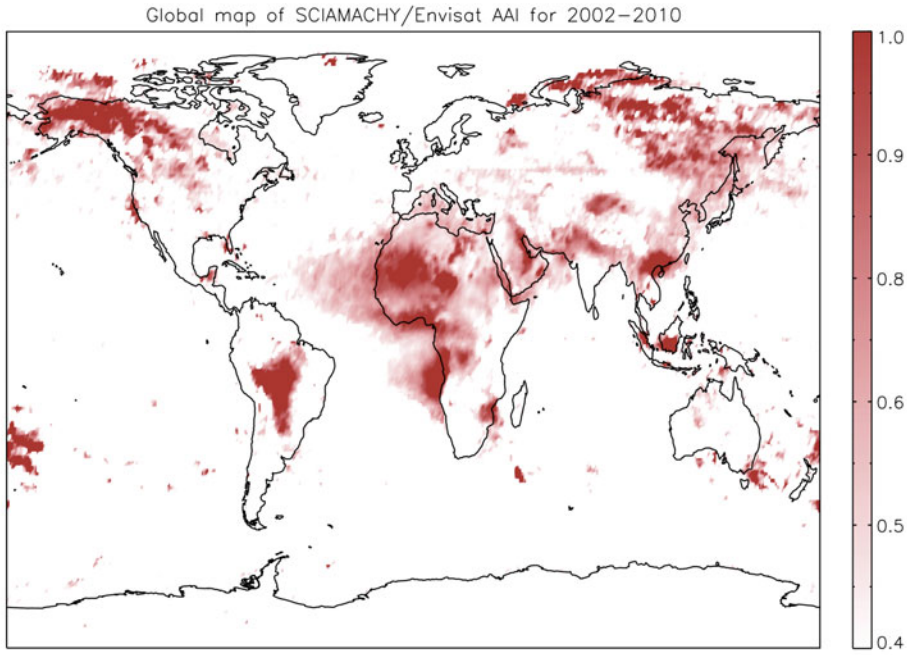

Figure 8.7 Global map of the Aerosol Index from SCIAMACHY, averaged over the period 2002-2010. The major UV-absorbing aerosol events are clearly visible, for example Saharan desert dust, Asian desert dust, biomass burning smoke in South-West Africa and South America, biomass burning smoke in South-East Asia, and smoke from wild fires in Siberia, Canada and Alaska. (Figure from L. G. Tilstra, KNMI).

8.7.2 Aerosol algorithm description and limitations

The main aerosol product from GOME is the UV absorbing aerosol index, AI (Chapter 7, Eq. 7.9). In the GOME application λ_0 (reference wavelength) is 380 nm and the λ is 340 nm.

The GOME AI was first used by Gleason et al. (1998) for a case study. The sensitivities of the AI to aerosol optical thickness, single scattering albedo, layer height, and other parameters are well documented (Torres et al., 1998; De Graaf et al., 2005). A global GOME AI product has been created.

Aerosol optical depth retrievals from GOME, using a standard multispectral least-squares fitting technique, have been performed by several groups (Torricella et al., 1999;

Veefkind et al., 2000; Kusmierczyk-Michulec and De Leeuw, 2005), but with limited success. The main problem is the large pixel size of GOME, which causes a high chance of cloud contamination. Sub-pixel cloud detection is not possible without additional information. Therefore, Holzer-Popp et al. (2002) used a combination of GOME with the ATSR-2 imager, but also in that case the number of useful pixels is very small. The use of the reflectance of the O_2 A-band measured by GOME for aerosol height retrieval was investigated by Koppers et al. (1997).

In the case of SCIAMACHY cloud contamination and uncertain surface albedo prevent accurate retrievals of τ (Von Hoyningen-Huene et al., 2007). However, the AI detects aerosols also in cloudy circumstances, whereas the surface albedo is low in the UV. Therefore, the AI is the most used aerosol product from SCIAMACHY (De Graaf and Stammes, 2005; Tilstra and Stammes, 2007). Figure 8.7 shows the global map of AI from SCIAMACHY, averaged over the period 2002–2010. The wide spectral range of SCIAMACHY has been used to analyze the complete reflectance spectrum of absorbing desert dust and biomass burning aerosols (De Graaf et al., 2007, 2012). Usually only positive values of the AI are being considered, which indicate absorbing aerosols. Negative values of the AI – i.e. scenes being bluer than aerosol-free scenes – from SCIAMACHY have been studied by Penning de Vries et al. (2009), showing a correlation with scattering aerosols.

The AI is the standard aerosol product for GOME-2, and as in the case of SCIAMACHY, the wavelength pair is 340/380 nm (Tilstra et al., 2010). As an improvement to GOME and SCIAMACHY, the Stokes parameter Q measured by GOME-2 will enable better characterization of aerosol microphysics, like particle size and refractive index. The planned retrieval method is based on fitting the modeled I and Q values to measured quantities in an optimal-estimation sense (Hasekamp and Landgraf, 2005a).

8.8 APS

8.8.1 Instrument description

The Aerosol Polarimetry Sensor (APS) was launched aboard the Glory satellite on March 4, 2011 but did not reach orbit due to the failure of the payload fairing to detach from the spacecraft. At the time of writing, it is unclear whether or not NASA will build and fly a copy of the APS instrument. Since APS data may never be available for the interested reader to evaluate, we will describe both APS and also an airborne instrument, the Research Scanning Polarimeter (RSP). The RSP instruments are airborne simulators of the APS, using the same measurement approach, and have been used to demonstrate the capability of that measurement approach to deliver reliable remote sensing observations with a polarimetric accuracy of ~0.1%. The RSP instruments have been flown in field experiments since 2001 and there are currently over 1000 hours of measurements available to the public that sample North and Central America from near the equator to close to the Pole.

The key measurement requirements for the accurate retrieval of a broad range of aerosol and cloud properties from photopolarimetric data are high accuracy, a broad spectral

range, and observations from multiple angles, including a method for reliable and stable calibration of the measurements. The polarimetric accuracy of the APS sensor is based on the use of Wollaston prisms to separate orthogonal polarization states from exactly the same scene at the same time and allows the required polarimetric accuracy of 0.2% to be attained even for scenes with sub-pixel heterogeneity. To measure the Stokes parameters that define the state of linear polarization (I, Q, and U), the APS employs a pair of telescopes. One telescope in the pair measures I and Q while the second telescope in the pair has the polarization azimuths of its measurements rotated 45° with respect to the first telescope so that it is measuring I and U.

In order to provide a broad spectral range, the APS uses three pairs of telescopes and in each telescope pair the light is split into three spectral bands for a total of nine spectral bands, in all of which the Stokes parameters I, Q and U are measured. The spectral bands are separated from one another using dichroic beam splitters and interference filters are then used to define each spectral channel. The APS measures wavelengths of 413, 555 and 866 nm in the first telescope pair, 444 (469 for RSP), 674 and 911 (962 for RSP) nm in the second telescope pair, and 1376 (1884 for RSP), 1603 and 2260 nm in the third telescope pair. Blue enhanced silicon detectors are used in the first two telescope pairs, but in order to provide sufficient sensitivity and low noise for observing aerosols over the oceans the detectors in the third telescope pair are made from HgCdTe and are cooled to 160° K. All spectral channels but the 911 (962) and 1376 (1884) nm ones are free of strong gaseous absorption. The 1376 (1884) nm exception is centered on a major water vapor absorption band and is specifically intended for detection and characterization of thin cirrus clouds. The 1884 nm band used by the RSP is better for cirrus cloud detection over snow and ice than the 1376 nm band, that is preferred for the APS, because of stronger ice absorption that makes the surface darker. However, for a satellite instrument a cirrus detection band at 1376 nm is better because of its capability to detect and characterize stratospheric aerosols with the accuracy required to simultaneously sense aerosols in the troposphere (Gao and Kaufman, 1992). The 910 (962) nm band provides a self-contained capability to determine column water vapor amount that is used to correct the longest wavelength bands (1603, 2260 nm) for contamination by water vapor. The locations of the other APS (or RSP) spectral channels are similar to those used in MODIS, MISR or POLDER and provide a wide spectral range (410–2260 nm) while minimizing the effects of absorbing gases.

The critical ability to view a scene from multiple angles is provided by scanning the 8 mrad APS instantaneous field of view (IFOV) along the spacecraft ground track with a rotation rate of 40.7 revolutions per minute (rpm) with angular samples acquired every 8 mrad. This yields ~220 useable view angles per scene over ±60° from nadir that are acquired over a 5-minute period as the spacecraft flies over the scene. The polarization-compensated scanner assembly includes a pair of matched mirrors operating in a “crossed” configuration such that polarized light that is incident “parallel” to the first mirror is “perpendicular” to the second mirror and vice versa. This type of scanner assembly has been demonstrated to yield instrumental polarization less than 0.05% and also allows a set of calibrators to be viewed on the side of the scan rotation opposite to the Earth. The APS calibrators provide comprehensive tracking of polarimetric calibration throughout each orbit, while radiometric stability was to be tracked monthly using lunar views. (The RSP is similar in many respects and in order to view a scene from multiple angles is oriented to

scan along the aircraft groundtrack. It has a rotation rate of 71.3 rpm, a 14 mrad IFOV and acquires samples every 14 mrad such that 150 views are obtained over ±60° with respect to nadir. To collect observations of a given scene at the ground over that view angle range takes about 5 minutes for an aircraft at 8.5 km altitude flying at 100 ms^{-1} similar to the time required to aggregate an APS scene.)

8.8.2 Aerosol retrieval algorithm description and limitations

The APS and RSP aerosol retrieval algorithms are essentially the same for clear-sky scenes, the only noteworthy difference being that calculations for an aircraft embedded in the atmosphere are somewhat more complicated than those for a satellite sensor. Since the APS sensor is not flying, we will therefore describe the algorithms currently being used in the analysis of RSP observations. The first step in preparing the observations for analysis is to correct them for ozone and nitrogen dioxide absorption which is assumed to lie above the tropospheric aerosols in the stratosphere and can therefore be corrected using Beer's law for the absorption in the path down to the aerosol layer and back to the observation point. The column water vapor is estimated from the reflectance ratio of a non-absorbing band (866 nm) and a band that has moderate water vapor absorption (911 nm) (Gao and Goetz, 1990) and is used to calculate an effective absorption optical depth for the 1603 and 2260 nm bands. Such an approximation is quite accurate because water vapor absorption is generated by the far wings of the absorption lines and absorption by carbon dioxide (1603 nm) and methane (2260 nm) in the lower atmosphere, where the interaction of absorption with aerosol scattering is important, is also dominated by line wings. The rapid attenuation of radiation in the upper atmosphere in the line centers that are contained in these spectral bands is included as a solar zenith dependent transmission correction (Cairns et al., 2003). Once the observations have been corrected for gaseous absorption effects the aerosol retrieval, whether over land or ocean, is based on an iterative adjustment of all the parameters required to define the surface and a bimodal aerosol model that minimizes the difference between the model and the measurements (Rodgers, 2000; Waquet et al., 2009b; Cairns et al., 2009; Dubovik et al., 2011; Hasekamp et al., 2011). The retrieved aerosol model consists of the effective radius, variance and spectral refractive index of each size mode and its optical depth with the accumulation, or fine, mode being restricted to effective radii smaller than 0.5 μm and the coarse mode consisting of aerosols with effective radii larger than 0.5 μm. If the residual fit between the observations and models is larger than expected based on a χ^2-test then a second retrieval is attempted using a nonspherical model for the coarse mode. At present we use a nonspherical model consisting of an equi-probable mix of prolate and oblate spheroids with aspect ratios from 0.3 to 3. We do not at present allow for a nonspherical accumulation mode because the differences between small spherical and nonspherical particles are relatively small and not readily detectable.

Over oceans the chlorophyll concentration ([Chl]) and windspeed define the ocean surface reflectance model, as discussed above, and are the surface parameters that are retrieved. The only difference between the ocean model used in the analysis of RSP measurements and the models of ocean reflectance described elsewhere in this chapter is the inclusion of polarization in the scattering of light within the ocean body and the calculation of the polarization of light emerging from the ocean. This is needed so that we have a complete and

consistent model of the contribution of the ocean to the observed unpolarized and polarized radiances (Chowdhary et al., 2006). The benefit of having such a model of the ocean body reflectance that only depends on [Chl] and predicts the oceanic contribution across the entire solar spectrum is that all of the APS unpolarized and polarized radiance observations from 410 to 2260 nm can be used in the aerosol retrieval. The value of being able to use the spectral bands across the visible part of the spectrum in aerosol retrievals is that the spectral shape of the ocean body contribution and the effects of aerosol absorption are very different and this difference allows an accurate determination of the single scattering albedo of the aerosols (Chowdhary et al., 2005). Size distribution and spectral optical depth retrievals over the ocean have also been validated during the Chesapeake Lighthouse Aircraft Measurements for Satellites (CLAMS) and the Megacity Initiative: Local and Global Research Observations (MILAGRO) field experiments (Chowdhary et al., 2005, 2011).

Over land the surface polarized reflectance is assumed to be grey (i.e., the same in all spectral bands) and has the same form, given by Nadal and Breon (1999) that is used in POLDER aerosols retrievals. The primary difference between the APS/RSP aerosol retrievals over land and the POLDER approach is that the pre-factor in the surface polarized reflectance model is estimated as part of the APS/RSP retrieval process. This surface parameter and the bimodal aerosol model parameters are the retrieval products over land. At present, only the polarized reflectance in all spectral bands is used in the aerosol retrievals over land. The advantage of only using the polarized reflectance is that the same method can be applied to aerosols over snow as well as other surfaces. This is possible because the polarized reflectance of snow is also grey and, although it has a smaller magnitude than is typical of other land surfaces, has a similar dependence on scattering angle to other surfaces types. Examples of retrievals over a range of conditions from very low aerosol optical depths to very high aerosol optical depths have demonstrated the capabilities of polarization observations over land including the capability to retrieve the aerosol single scattering albedo (Waquet et al., 2009b; Knobelspiesse et al., 2011) which complements the capability to determine aerosol absorption in the UV that was presented in Section 8.5.

One of the main limitations of the existing analysis approach over both ocean and land surfaces is that the iterative estimate is relatively slow because the calculation of how the polarized radiation field varies as a function of all the aerosol and surface parameters is performed using direct numerical differentiation. Hasekamp and Landgraf (2005b) have shown that perturbations to the radiation field as a function of surface and aerosol parameters can be calculated analytically and we are currently testing an implementation of that approach using our own radiative transfer code. Our own code uses the doubling/adding method, which has the advantage for the analysis of multiangle observations that the effect of any possible perturbations on all view angles can be evaluated using a single radiative transfer calculation. In addition, comprehensive look-up tables are also being tested as a quicker method for initializing the iterative search.

An issue regarding the aerosol retrievals over land is the generality and accuracy of the existing surface polarization models (Maignan et al., 2009; Litvinov et al., 2011) such as that of Nadal and Breon (1999) and may be a particular problem at high scattering angle for snow surfaces. Although we have found our equi-probable shape distribution approach to modeling dust and soil to work for far travelled dust off the coast of Virginia and soils blown off the coast of Mexico other models of dust may be required such as that used in

the AERONET retrievals (Dubovik et al., 2006). Lastly, although the use of only polarized reflectance to perform aerosol retrievals over land allows for a relatively simple algorithm and the multiangle polarization observations in long wavelength bands at 1603 and 2260 nm do provide some sensitivity to coarse mode aerosols, the inclusion of unpolarized reflectance observations in the retrieval of aerosols over land from POLDER observations has been demonstrated by Dubovik et al. (2011) to have significant benefits and we plan on implementing a similar retrieval approach in future analyses of the RSP data sets.

8.9 Advances in remote sensing of aerosol using modern sensors

The previous sections have presented a survey of many sensors and algorithms used for aerosol retrievals during the 2000s and beyond. All of the algorithms presented in previous sections are more or less "standard algorithms", supported by various space agencies to provide aerosol information to the public. The algorithms were developed over a number of years and applied to the sensors at launch. There have been changes since launch, and some of those changes have been major. For example, the MODIS Deep Blue algorithm was implemented five years after Terra launch. However, change comes slowly. While the standard algorithms continue to produce a continuous time series of important aerosol products, research into how to extract even more information by applying new techniques is taking place. In this section, we introduce some recent advances in aerosol remote sensing applied to the observations from the passive sensors described above. Some of these techniques may eventually be included in the operational algorithms.

8.9.1 Aerosol retrieval over clouds

One characteristic that all sensors and retrieval methods described above have in common is that they retrieve aerosol only in cloud-free scenes. This severely limits true global coverage of aerosol properties and misses the ability to quantify possible positive aerosol forcing when dark aerosol is lofted above clouds (Chand et al., 2009). Two techniques for retrieving aerosol optical depth above clouds have been developed over the last few years. The aerosol load above clouds can be retrieved from observations of polarized radiances as described by Waquet et al. (2009a) and Knobelspiesse et al. (2011), and from radiance measurements in the near UV (Torres et al., 2011).

The Polarization method

One of the observations of cloud top pressure (CTP) from PARASOL, a standard PARASOL data product, makes use of the polarized reflectance. Since the polarized reflectance at 0.49 μm increases with the "thickness" of the molecular atmosphere, an apparent cloud top pressure called "Rayleigh CTP" (Goloub et al., 1994) can be derived from the value of the polarized reflectance. The presence of an aerosol layer mixed with molecules above a cloud changes the polarization at 0.49 μm and makes the cloud higher than it would be in the absence of aerosols. So, in such conditions, inconsistencies occur with the second PARASOL CTP based on differential absorption measurements in two oxygen A-band channels at 0.76

μm (Vanbauce et al., 2003) or with the MODIS "IR CTP" in the thermal infrared channels when available (Menzel et al, 2008) that are not affected. Let us state that discrepancies are anticipated between the three CTPs (Sneep et al., 2008) since the retrievals are based on different physical processes that are not exactly sensitive to the same altitude range, but when the "Rayleigh CTP" over some regions is smaller than the two others, it is in conflict with our understanding.

Such observations (Waquet et al., 2009b) were noticed from PARASOL in areas located in regions and times associated with the presence of aerosols in the fine mode, i.e. with pollution and/or smoke generated mainly by anthropogenic activities. Several cases have been investigated over the subtropical South Atlantic ocean in August/September when fires in Southwest Africa are frequent and meteorological processes favor biomass burning aerosol transport to the West. Waquet et al. (2009b) analyzed specific collocated POLDER/PARASOL, MODIS and CALIOP observations in 2006, from 14 to 18 August and found an "additional" polarization signal over the 90°–120° scattering angle range. This additional polarization leads the "Rayleigh" algorithm to an underestimate of the CTP confirmed by the CALIOP data. The excess of polarization is due to the presence of an aerosol plume, as also confirmed by CALIOP observations. Modeling the radiative transfer through the cloud-aerosol atmosphere can then retrieve the aerosol optical thickness ($\tau_{aerosol}$). Presence of dust cannot be detected with a similar approach since the dust polarization is not significant, but a method using the polarized rainbow is an alternative under development (Waquet el al., 2010).

Similar observations of aerosols above cloud were made by the RSP as part of the Megacity Initiative: Local and Global Research Observations (MILAGRO) field campaign on March 13, 2006. In this case, the presence of aerosols was identified as a result of the inconsistency between cloud top pressure estimates using polarized reflectance measurements in spectral bands at 0.41 and 0.469 μm. The aerosol layer was lofted above a low altitude marine stratocumulus cloud close to shore in the Gulf of Mexico. The analysis approach used with these aircraft observations is to first determine the cloud droplet size distribution using the angular location of the cloud bow and other features in the polarized reflectance. This cloud retrieval is then used in a multiple scattering radiative transfer model optimization to determine the aerosol optical properties and the cloud droplet size distribution using only the polarized reflectance observations over the spectral range from 0.41 to 2.260 μm. This approach is taken because the cloud optical depth does not then need to be estimated since the polarized signal generated by a cloud saturates at an optical depth of 2–3. The retrieved aerosol variables are the aerosol optical depth, the fine mode aerosol size distribution and its complex refractive index (Knobelspiesse et al., 2011). Subsequent unpublished analysis demonstrates that the imaginary refractive index can be retrieved far more accurately by including total reflectance observations in the optimization process and also retrieving the cloud optical depth, similar to what is discussed in greater detail in the next subsection.

The near UV method

This retrieval technique uses observations of backscattered near-UV reflectance observed by the OMI sensor on the Aura satellite. The retrieval requires both the OMI-derived absorbing Aerosol Index and the observed 0.388 μm reflectance, which are fed into an inver-

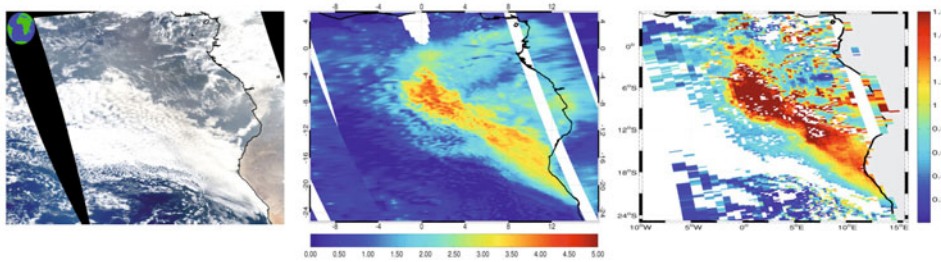

Figure 8.8 Stratocumulus cloud as seen by Aqua-MODIS (left), OMI observed Aerosol Index (center), and derived aerosol optical depth above the cloud (right).

sion procedure that simultaneously retrieves the optical depth of both the cloud and the aerosol above the cloud. Sensitivity analysis studies (Torres et al., 2011) indicate that the magnitude of the Aerosol Index associated with absorbing aerosols above clouds depends on cloud and aerosol optical depth, wavelength-dependent aerosol single scattering albedo and, to a lesser extent, on aerosol layer-cloud separation. Thus, to simultaneously retrieve $\tau_{aerosol}$ and τ_{cloud}, knowledge of other cloud and aerosol parameters is needed. An error analysis was carried out to estimate the uncertainty in the retrieved values of aerosol and cloud optical depth associated with the uncertainty in the assumed values of single scattering albedo and aerosol cloud separation. Results indicate that the combined uncertainty of ±0.03 in single scattering albedo and ±2km in aerosol-cloud separation yields a $\tau_{aerosol}$ error between −26% and 54% for typical cloud and aerosol layer optical depths of 10 and 0.5, respectively. Retrieval errors decrease with increasing cloud optical depth. Errors in retrieved τ_{cloud} are smaller than 20% in most cases which are comparable to the reported uncertainty of the MODIS product for optical depths larger than about 10 (Platnick et al., 2003).

An example of the application of the UV method of above-cloud-aerosol optical depth retrieval is shown in Figure 8.8. The left panel shows the MODIS-Aqua true color image composite of a horizontally extended stratocumulus cloud over the South Atlantic Ocean off the coasts of Namibia and Angola on August 4, 2007. The center panel illustrates the OMI Aerosol Index indicating the unmistakable presence of an absorbing aerosol layer overlying the stratocumulus cloud. The right panel depicts the aerosol optical depth field derived by the UV technique.

8.9.2 The MAIAC retrieval

The standard MODIS aerosol products described above, both Dark Target and Deep Blue, are applied to the data collected on each orbit, soon after that orbit's data are downloaded from satellite to processing center. The retrieval is completely independent of observations taken yesterday or tomorrow, except in terms of using long-term means or climatology as ancillary data.

The Multiangle Implementation of Atmospheric Correction (MAIAC) algorithm (Lyapustin et al., 2011a) was designed for simultaneous retrievals of aerosol information and surface bidirectional reflectance over land. To achieve this goal, it uses a time series analysis of images from multiple days and simultaneous processing for groups of 25×25 1 km^2 pixels, called blocks. In this way, the processing accumulates enough measurements to exceed the number of unknowns – the necessary condition for solution of the inverse problem. This method relies on different space-time scales of variability of aerosol and land reflectance: namely, the land surface is variable in space but changes little over short time intervals, while the aerosol is homogeneous across a spatial domain of ~25 km but can change rapidly from one day to the next.

MAIAC stores in memory from 16 days of measurements over the equator to five days at the Poles, and implements a sliding window algorithm. The surface BRDF is characterized by the linear Ross-Thick Li-Sparse BRF model (Lucht et al., 2000) depending on three parameters, which are derived for each pixel from up to 16 observations at different view angles acquired on different days. The multi-day block-level processing is used to derive spectral regression coefficient (SRC) for each pixel which relates BRF in the Blue and shortwave infrared (SWIR, 2.13 μm) bands. The inversion is simplified by an assumption of spectral invariance of the BRF shape (Veefkind et al., 1998; Diner et al., 2005), which works well over dark and moderately bright surfaces. Once SRC is known, the BRF in the Blue band (B3) is computed at 1 km resolution as a product of SRC and BRF in the SWIR band. This allows MAIAC to derive aerosol information at 1 km resolution using the latest MODIS measurements.

The MAIAC aerosol algorithm applies a look-up table approach (LUT) (Lyapustin et al., 2011b) to computing top-of-atmosphere reflectances in reflective MODIS channels. Similar to the standard MODIS land algorithm, the aerosol models are prescribed by region and season. Unlike the standard algorithm, the models are tuned on a local level in order to achieve a good agreement of spectral MAIAC τ with AERONET measurements. Also unlike the standard over land algorithm, the prescribed fine and coarse models are monomodal lognormals, not multimodal models, and MAIAC combines the designated fine and coarse modes using the η parameter much like the standard MODIS over ocean technique (Section 8.2.2 and Equation 8.4),. MAIAC obtains an assessment of physical size parameter information over land, unlike the standard over land retrieval, because the temporal information fixes the surface contribution and reduces the overall uncertainty; however, the accuracy of retrieving Ångström parameter by MAIAC remains low (Lyapustin et al., 2011a).

MAIAC's assumptions are met over dark and moderately bright surfaces. Over deserts, an alternative retrieval path is implemented, including an additional dust aerosol model in the LUT and an empirical correction factor for the angular dependence of SRC which

becomes prominent over bright surfaces. Results over bright surfaces are promising, but still in development.

MAIAC retrieval of aerosol optical depth compare as well with AERONET observations as the standard MODIS land algorithm over dark and vegetative surfaces (Lyapustin et al., 2011a), but at 1 km spatial resolution instead of 10 km. There is also evidence that MAIAC produces a more accurate retrieval in some regions that have been difficult for standard retrieval, including western North America. Recently, MAIAC was applied to MODIS observations over the European Alps in order to obtain a finer resolution product that could resolve aerosol gradients and particulate pollution in narrow Alpine valleys. After some specialized filters were applied to the results to account for residual snow and cloud contamination, the results proved to be useful (Emili et al., 2011).

From a historical perspective, MAIAC's development was strongly influenced by the extensive heritage of the MISR and MODIS retrieval algorithms. Influences include employing a rigorous radiative transfer model with a non-Lambertian surface for simultaneous aerosol/surface retrievals (Diner et al., 2001), the concept of using the image spatial structure for aerosol retrievals over land (Martonchik et al., 1998) and the Contrast Reduction method by Tanré et al. (1988) that showed that consecutive images of the same surface area, acquired on different days, can be used to evaluate aerosol differences between days (Section 7.4.3).

8.9.3 Single scattering albedo using critical reflectance methods

Aerosol absorption, as denoted by the single scattering albedo, is an important particle property to retrieve. MISR is able to use its multiangle capability to retrieve ϖ under the right conditions, and OMI is sensitive to aerosol absorption in the UV range of the spectrum where aerosol absorption introduces a deviation from expected Rayleigh scattering. MODIS produces a ϖ through its Deep Blue pathway, based on similar principles as OMI. The PARASOL advanced retrieval will obtain this parameter using multiangle and polarization information. There is an alternative method to obtain aerosol absorption information using MODIS. This method does not require polarization, multiangle looks or Deep Blue channels and can be applied to any wavelength as long as there is sufficient aerosol loading in that wavelength. This is the critical reflectance method.

When a scattering aerosol overlays a dark surface, the reflectance measured at the top of the atmosphere will be greater than without the aerosol because the particles are scattering sunlight back to space. The particles prevent the surface below from absorbing some of that sunlight. The more aerosol added to the scene, the more light scattered, the higher the measured reflectance at top-of-atmosphere. If the aerosol were an absorbing aerosol with low single scattering albedo and the underlying surface was bright, then the reflectance measured at the top of the atmosphere would be less than without the aerosol. In this case, the particles are absorbing the sunlight that would otherwise be reflected by the bright surface back to space. The more aerosol in this case, the more absorbed light, the lower the reflectance at top-of-atmosphere. An example of the interplay between aerosol absorption and underlying surface is illustrated in Figure 1.1, where the underlying surfaces are dark ocean and bright cloud. Thus, between these two situations there exists a combination of surface brightness and aerosol absorption properties in which adding more aerosol makes

no change to the measured reflectance at top-of-atmosphere. This point is called the "critical reflectance" (Fraser and Kaufman, 1985). If the surface reflectance is constant, then the critical reflectance is determined solely by the aerosol properties and is most sensitive to the absorbing properties of the particles. Therefore, critical reflectance provides a remote sensing technique to derive aerosol single scattering albedo (Kaufman, 1987; Kaufman et al., 1990; 2001; Zhu et al., 2011).

The practical crtical reflectance remote sensing algorithm requires two images of the same scene with nearly the same solar and viewing geometries. If the aerosol loading did not change from image to image and the surface reflectance also did not change, a scatter plot of top-of-atmosphere reflectances of one image against the other would have all pixels aligned along the 1:1 line where $x=y$. However, if the aerosol loading did change while the surface remained constant, then plotting the hazier day against the clean day would create a scatter plot in which the pixels would align linearly, but not on the 1:1 line. For darker surfaces and a scattering aerosol, the hazier pixels would have higher values than the corresponding pixels of the clean day. For brighter surfaces and a more absorbing aerosol, the hazier day would darken the top-of-atmosphere reflectance and appear below the 1:1 line on the scatter plot. The point at which the line created by the hazier pixels intersected the 1:1 line would be the critical reflectance. Single scattering albedo (ϖ) could be derived from look-up Tables (LUTs) that relate ϖ to critical reflectance for a particular set of scattering properties (size distribution and real part of the refractive index) for the type of aerosol in question (Zhu et al., 2011; Wells et al., 2012).

The critical reflectance method has been applied to MODIS reflectances to derive spectral ϖ in smoke (Zhu et al., 2011) and dust (Wells et al., 2012), at moderately high spatial resolution. There are limitations to the method that have been explored in sensitivity studies, but the final product shows agreement with AERONET retrievals of ϖ to within 0.02 (Zhu et al., 2011; Wells et al., 2012).

8.9.4 Aerosol plume heights

One additional capability made possible by the multiangle MISR imaging is the retrieval of wildfire smoke, volcanic effluent, and desert dust plume heights (Kahn et al., 2007). The technique, based on interpreting the parallax in terms of elevation above the geoid, requires features in the aerosol plume to be matched in the multiangle views (Moroney et al., 2002; Muller et al., 2002); as such, this technique can be applied primarily within a few hundred kilometres of aerosol sources, where aerosol plumes are well defined. However, height maps of entire near-source regions are routinely produced, and the stereo imagery provides global coverage approximately once per week, so climatologies of smoke, dust, and volcanic plumes are contained in the 11-year MISR data record.

MISR aerosol plume heights are complementary to the CALIPSO active sensor aerosol profile retrievals (Chapter 10), which provide only very narrow-swath (~70 m) "curtain" coverage and rarely, if ever, capture active sources, but are sensitive to aerosol layers as optically thin as 0.005 (Winker et al., 2009). Thus MISR data can be used to constrain aerosol injection heights and near-source plume evolution, whereas CALIPSO lidar can provide aerosol elevation downwind, when the plumes have dissipated into much more extensive, sub-visible layers, the combination offering powerful constraints on aerosol transport modelling (Kahn et al., 2008).

The MISR Stereo Height algorithm also includes a wind correction, which makes use of cloud motions observed with the steeply viewing MISR cameras; the heights are then retrieved by the automatic algorithm using the near-nadir cameras, to limit the relative distortion and improve stereo matching (Moroney et al., 2002). An interactive computer tool has also been developed which provides more detailed height and wind information on individual plumes than is available from the operational algorithm (Nelson et al., 2008). A database of plumes digitized with this tool can be found at: http://misr.jpl.nasa.gov/getData/accessData/MisrMinxPlumes/index.cfm. Early work with the MISR plume height products has demonstrated that smoke from wildfires can be injected above the atmospheric boundary layer, which means it will stay aloft longer, travel farther, and have broader environmental impact than is often assumed in aerosol transport model simulations (Kahn et al., 2007; Mims et al., 2009; Val Martin et al., 2010).

8.9.5 Advances using combination of sensors or sensors and models

One of the most important innovations in aerosol remote sensing occurring during the 2000s is the placement of multiple instruments on the same platform or formation flying satellites so that the strengths of different instruments could complement each other for more comprehensive understanding of the aerosol system. The Terra satellite includes both MODIS and MISR so that they view some of the same scenes simultaneously. The A-Train is a constellation of satellites that follow the same orbit and allow views of the same scene within minutes of each other. Of the sensors described above, Aqua-MODIS, Aura-OMI and PARASOL-POLDER have all flown in formation as part of the A-Train. Also included in the A-Train is the active sensor, CALIPSO-CALIOP, described in Chapter 10.

Combining information from different sensors can take various forms. Most common are the studies that use different products from different sensors to answer scientific questions. For example, cloud-aerosol studies might use MODIS aerosol optical depth and particle size parameter, MODIS cloud optical properties, CALIOP vertical profiles of aerosol and clouds, and other sensors in the A-Train providing information on chemistry, clouds and precipitation (Yuan et al., 2011, among many). In a similar way, MISR smoke plume heights and aerosol optical depth have been used in conjunction with MODIS fire radiative power to enhance our understanding of plume rise from fires (Val Martin et al., 2010). Kalashnikova and Kahn published in 2008 an excellent exploration of the complementary contribution that could be obtained by combining the information from two sensors. In this work, MISR images were used to fill the gaps left by sun glint in the MODIS over ocean retrieval to better track the evolution of desert dust across the Atlantic ocean. Use of the MISR data increased the MODIS coverage by 50%. In addition, the paper notes that MODIS provides the necessary coverage to track plumes that are difficult for MISR's narrower swath to resolve, but that MISR provides measures of particle properties that are essential to identify dust and quantify the evolution of particle size and ϖ as the plume is transported. The two sensors together provide a much clearer picture of dust transport than would be obtained from either one working alone.

A step beyond using standard archived products together to answer specific science questions and provide complementary views of the aerosol system is to use information from one sensor to constrain assumptions within the retrieval of another sensor. Joint re-

trievals can include passing cloud mask information from a moderate spatial resolution instrument such as MODIS or MISR to a coarser resolution instrument such as OMI or POLDER, or using retrieved particle property information from MISR or POLDER back to MODIS or OMI to constrain choice of aerosol model in the retrieval's LUT. An example of a joint retrieval is found in Satheesh et al. (2009) where MODIS retrieved τ is used to constrain the assumptions in the OMI retrieval, allowing for a more accurate retrieval of ϖ. The section above entitled "Near UV aerosol algorithm (OMAERUV)" describes the OMAERUV retrieval of τ and ϖ. The sensitivity of the retrieval to aerosol layer height is noted, which is constrained operationally by assuming climatological values for aerosol height. In the joint OMI-MODIS retrieval, MODIS provides τ, reducing the number of unknowns in the OMI retrieval, which then returns ϖ and a retrieved (not climatological) aerosol layer height.

Finally, much clarity of the aerosol system can be obtained by combining satellite remote sensing products with numerical models, either by constraining model output that encourages modification of model assumptions and parameterizations, or by active assimilation of aerosol products resulting in hybrid model-observation depictions of the aerosol system. Such assimilated data sets are becoming more commonplace and are shown to be an improvement to model-only generated aerosol fields (Zhang et al., 2008; Benedetti et al., 2009). These assimilated fields remove some of the biases in the satellite products and fill in holes in the retrieved fields due to clouds, sun glint, inappropriate surfaces, etc.

8.10 Summary

The 21st century has seen an explosion of space-based passive aerosol remote sensing using sensors that make use of all aspects of the radiation field: direct solar attenuation through the atmosphere, wide spectral range, multiangle views, fine spectral resolution in the ultraviolet spectrum and polarization. This has spawned a wide variety of responses as different development teams have worked to extract as much information as possible from the measurements of each particular sensor. Each sensor has strengths that allow for specific capabilities in terms of aerosol retrievals and each sensor has limitations. Table 8.2 summarizes these strengths and limitations.

Ideally, the perfect passive aerosol satellite sensor would have broad swath coverage, pixel spatial resolution of less than 1 km, a spectral range stretching from the UV to the mid-infrared, multiple angle views of the same scene and highly accurate polarization in all channels. Such an instrument does not exist now, but a combination of information from different sensors does increase capability, and also aids in the important effort of characterizing uncertainty in the products and keeping an eye on calibration drifts.

The 21st century continues to be a golden era for passive shortwave aerosol remote sensing. The constellation of satellite sensors observing Earth is supplying unprecedented aerosol information. This fleet of instruments provides an important global perspective that complements the more local focus of ground-based instruments. Still, these instruments observe aerosol only during daylight and provide only total column measures through the

lower atmosphere. The complete picture of the aerosol system requires IR and lidar techniques that offer nighttime views and vertical profiling.

Instrument	**Swath width (km)**	**Pixel resolution – nadir (km)**	**Wavelength range (μm)**	**Number of wavelengths**	**Angular range**	**Number of angles per scene**	**Polarization**
SAGE(s)			0.38–1.55	4 to 9			
MODIS	2330	0.5x0.5	0.41–2.13	8 for aerosol	±70°	1	none
MISR	380	0.275 x 0.275 to 1.1 x 1.1	0.446–0.866	4	70.5° aft to 70.5° forward	9	depolarized
POLDER	1600	5.3 x 6.2	0.443–1.020	7 for aerosol	±43° across track ±51° along track	14–16	in 3 channels, I,Q,U
OMI	2600	13 x 24	0.27–0.50	Hyper-spectral	±70°	1	none
GOME	960	40x320	0.24–0.79	Hyper-spectral	±30°	1	limited
SCIAMA-CHY	960	30x60	0.24–2.3	Hyper-spectral	±30°	1	limited
GOME-2	1920	40x80	0.24–0.79	Hyper-spectral	±55°	1	Q/I
APS	6	6x6	0.41–2.26	7 for aerosol	±60°	220	all channels I,Q, U

Table 8.2 Comparison of instrument capability for selected passive shortwave sensors producing aerosol products in the 2000s.